

In This Issue:



Articles

The Temperature Dependence of Spectral Broadening in the Hg ($6^1S_0 - 6^3P_1$) Multiplet At High Optical Densities	Walter Braun, Milton D. Scheer, and Victor Kaufman	313
Absolute Isotopic Abundance Ratio And Atomic Weight Of a Reference Sample of Gallium	L. A. Machlan, J. W. Gramlich, L. J. Powell, and G. M. Lambert	323
Thermal Expansion of Platinum And Platinum-Rhodium Alloys	R. E. Edsinger, M. L. Reilly, and J. F. Schooley	333

News Briefs and Reports

New Technical Developments	357
New Standard Reference Data	359
New Services From NBS	359
New Standard Reference Materials	360
Report: I-R 100 Winners	360

The Temperature Dependence of Spectral Broadening in the Hg ($6^1S_0-6^3P_1$) Multiplet At High Optical Densities

Volume 91

Number 6

November-December 1986

**Walter Braun,
Milton D. Scheer, and
Victor Kaufman**

National Bureau of Standards
Gaithersburg, MD 20899

A new method has been developed for determining rapidly changing translational temperatures in a gas that has been heated by such transient phenomena as the passage of a shock wave or the absorption of sub-microsecond pulses of radiation from an infrared laser. The method depends upon the use of trace amounts of Hg vapor and its absorption of radiation in the neighborhood of the 253.7 nm isotopic and hyperfine multiplet. As the Hg atoms sense changes in the translational temperature of the host gas, the absorption of 253.7 nm radiation also changes by virtue of the Doppler and Lorentz broadening of the multiplet lines. Emission spectra of a Hg discharge light source in the neighborhood of 253.7 nm were shown to be

readily simulated by a two zone computer model even at large optical densities. The same lamp parameters that were used in these calculations could also be used to simulate the experimental pressure and temperature dependence of the total integrated absorption. This provided a means for obtaining the temperature calibration curves needed to monitor the changing translational temperature of a gas undergoing rapid heating or cooling.

Key words: absorption; atoms; calibration; Hg; lamp; line profile; radiation; resonance; temperature dependence; transient heating.

Accepted: July 10, 1986

1. Introduction

A new method for determining transient translational gas temperatures has been developed. It involves the use of small concentrations of Hg atoms to monitor the translational energy associated with molecules of the host gas. For example, after undergoing rapid vibrational excitation, the host molecules collisionally equipartition the deposited energy and the monatomic Hg tracer senses the increase in translational temperature. Such vibra-

tional excitations are usually achieved by the absorption of a laser pulse either in the ultraviolet (electronic excitation followed by rapid internal conversion to the ground electronic state) or directly by absorption of an intense laser pulse in the infrared. The passage of a shock wave through the gas on the other hand, rapidly increases the translational temperature so that the process of equipartition results in an increase in rotational and vibrational energies and is accompanied by the net decrease in the translational temperature which the Hg atoms monitor. The relaxation time constants for these processes provide a means for directly determining the efficiency with which energy is transferred between molecules by collisional processes.

About the Authors: Walter Braun and Milton D. Scheer are with the Chemical Kinetics Division and Victor Kaufman is with the Atomic and Plasma Radiation Division in NBS' National Measurement Laboratory.

A Hg atom can be used to detect changes in the translational temperature of a surrounding gas by noting the quantitative features of the absorption spectrum in the neighborhood of the resonance transition at 253.7 nm ($6^1S_0-6^3P_1$). This spectrum is complex because of the natural isotopes of Hg and the hyperfine structure of the odd numbered ones. The absorption of radiation in this region changes with translational temperature due to Doppler and Lorentz (collisional) line broadening. It will be shown that both the pressure and temperature dependence of the absorption can be calculated by matching the high resolution spectrum of the light source with a computer model that takes into account both the Doppler and Lorentz effects [1].¹

It has been shown previously that a simple two zone model can simulate the light emission from an atomic resonance lamp [2]. This representation is superior to earlier methods [1] in that actual lamp temperatures are used rather than unrealistically high ones that are chosen primarily to represent different emitting and absorbing atom densities in the lamp. In the two zone model, zone 1 is assumed to contain both emitting and absorbing atoms uniformly distributed. The emission from this zone, at the frequency ν_r , is proportional to the emittance: $J_1(\nu_r)$, which is given by the expression

$$J_1(\nu_r) = 1 - \exp(-k_1(\nu_r)). \quad (1)$$

The Napierian absorption coefficient $k_1(\nu_r)$, for a Lorentz broadened Doppler line is defined in the appendix. The second zone, which is assumed to contain only ground state Hg atoms, absorbs some of the radiation from zone one and transmits radiation proportional to the emittance. Therefore $J_2(\nu_r)$ is given by

$$J_2(\nu_r) = J_1(\nu_r) \exp(-k_2(\nu_r)). \quad (2)$$

This quantity is proportional to the radiation emitted by the lamp so that when it is attenuated by an absorption cell containing Hg vapor, the transmitted radiation intensity is proportional to its emittance $J_2(\nu_r)$, namely

$$J_3(\nu_r) = J_2(\nu_r) \exp(-k_3(\nu_r)), \quad (3)$$

where the subscript 3 distinguishes this externally absorbing region from the lamp zones 1 and 2.

Such a two zone model description of the lamp provides a simple means of representing the actual

gradients in absorber and emitter concentrations that are always present in any lamp configuration. The results obtained with models containing more complex distributions of the absorbing and emitting atoms have been shown to be virtually indistinguishable from the idealized two zone model [3].

In earlier work [4] lamps were constructed, and emission profiles obtained, in order to determine the concentration dependence of either fluorescence or absorption signals in zone 3. In these instances optically thin lamps were used to maximize the detection sensitivity for the fluorescing and absorbing atoms. Since optically thin lamps contain low pressures of inert buffer gas, line profile simulations were made invoking Doppler broadening only. These simulations were compared with experiment either by matching the computed and observed absorption vs. concentration calibration curves (curve of growth method) [5], or by matching computed emission profiles with high resolution emission spectra of the lamp (direct method) [6,7].

In the present work we have used the resonance absorption phenomenon to determine transient translational temperatures over a wide dynamic range. The two zone model was extended to very large optical depths (>1000), using all of the multiplet components of the Hg resonance line with only Doppler and Lorentz broadening effects incorporated into the computations.

2. Experimental

Two types of resonance lamps were used. An unreversed lamp with a low value of optical depth was constructed by placing a drop of mercury in a 12 mm o.d., 15 cm long quartz tube which had been previously evacuated and baked. After addition of the mercury, the tube was evacuated again, filled with argon to a pressure of about 4 Torr and sealed. An electrodeless, microwave (~ 2.5 GHz) discharge was initiated and maintained at 5 watts. After the discharge stabilized, the lamp assembly was cooled with a stream of compressed air and the radial emission focused onto the entrance slit of a spectrograph with a resolution of 1.6×10^6 . Under microdensitometer examination the exposed photographic plates showed five very narrow, unreversed Hg multiplet lines in the neighborhood of 253.7 nm.

A second lamp, suitable for operation at large optical depths, consisted of a commercial, single ended, pencil-like lamp that contained a drop of mercury in about 100 Torr of argon. It consisted of

¹ Figures in brackets indicate literature references.

a dual bore fused silica tube 5.4 cm long and 6 mm o.d. with both electrodes mounted and sealed at one end. Power for the lamp was supplied by a filtered dc power supply (450 volts) in series with a current regulating circuit. The lamp current was adjustable between 5 and 20 mA without significant destabilization at the low current extreme. A hollow brass cylinder 16 mm o.d., 10 mm i.d., and 8 cm long was used as a heat sink and enclosed the lamp assembly. A 3 mm hole was drilled perpendicular to the cylinder axis and served as a collimating aperture for the light source. Stable operation required a constant lamp temperature since a change of one degree resulted in about a 15% change in Hg pressure and hence in the lamp's optical depth. As a result good voltage and current regulation of the power supply, and high thermal stability of the lamp were found to be necessary for satisfactory absorption measurements to be made.

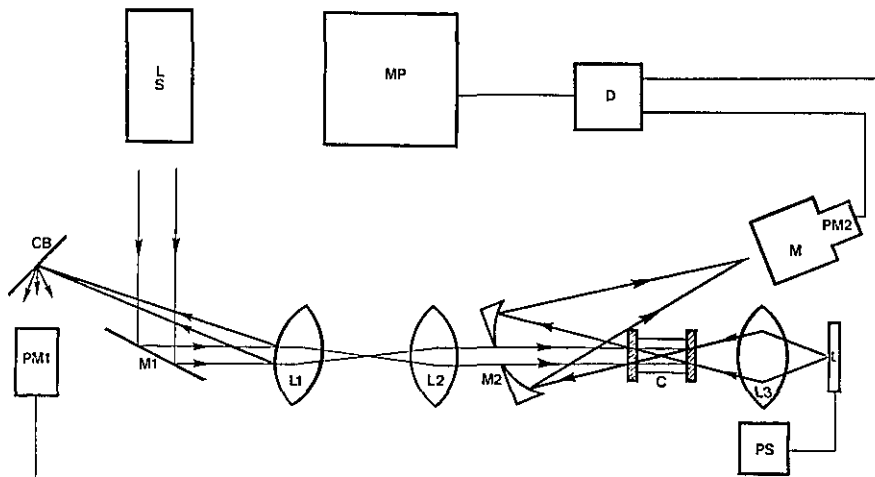
The high resolution lamp spectra were photographed with Kodak SWR spectroscopic plates that were calibrated by exposure at constant density for known times and examined with a microdensitometer so that plate density-exposure curves could be obtained. These showed the expected departure from reciprocity at short exposures, saturation at long exposures, and linear behavior over a considerable range of median exposures.

Absorption measurements were performed as follows: the high optical density Hg lamp was partially focused through the center of a Hg-containing absorption cell that was 5 cm long. The emerging beam was focused onto the entrance slit of a low resolution f/6 grating monochromator set at 253.7 nm with a 1P28 photomultiplier positioned at the exit slit. The output of the photomultiplier was connected to a preamplifier whose input

impedance was 1000 ohms and whose 50 ohm output impedance was matched to the input of a digitizer that was set in a continuous sweep mode. For a known gain of the digitizer's input amplifier, a digitized voltage offset could be adjusted to null the constant signal displayed on an oscilloscope. The value of this offset voltage (S_0) was proportional to the intensity of the lamp. When 1.8 mTorr of Hg (vapor pressure at 298 K) was introduced into the absorption cell, the null point shifted to a lower value of the offset voltage (S_1) which is proportional to the light intensity reduced by the Hg absorption. Thus the fraction of the 253.7 nm radiation absorbed is given by $(S_0 - S_1)/S_0$. The accuracy of this quantity is limited primarily by the signal noise and the 1% resolution of the offset control. Longterm stability, as determined by a set of successive absorption measurements, was found to vary within $\pm 2\%$ of the mean. The linearity of the detection system was verified by attenuating the 253.7 nm beam with calibrated neutral density filters.

The apparatus, shown schematically in figure 1, was used to monitor transient temperature excursions. A CO₂ TEA laser irradiated the absorption cell which contained a trace of Hg vapor and an infrared absorbing gas such as SF₆. Pressures were measured with a capacitance manometer. A fraction of the laser beam was reflected from the front surface of the first lens and focused onto a carbon block. A visible incandescent light pulse with a 50 ns rise time was thus produced and triggered the digitizer. The output signal was computer averaged for as many sweeps as was necessary to produce a satisfactory signal to noise ratio. Absorption of the resonance radiation by Hg vapor could thus follow temporal changes in the translational temperature of gases in the absorption cell.

Figure 1—Schematic diagram of the apparatus used to transiently heat SF₆ and to measure its translational temperature. LS is the CO₂ TEA laser; M1 is a reflecting mirror; L1 is a partially reflecting tilted lens; L2 is a collimating lens; M2 is a split, curved mirror with the center section removed; C is a narrow bore absorption cell containing BaF₂ windows (connection to vacuum line not shown); L3 is a lens for focusing radiation from the Hg resonance lamp L; PS is a regulated DC power supply; M is a low resolution f/6 monochromator; PM2 is a 1P28 photomultiplier; D is a fast digitizer; MP is a microcomputer; CB is a carbon block that incandesces when irradiated by the CO₂ laser and is used to trigger the digitizer by means of the photomultiplier PM1.



3. Results and Discussion

3.1 The Hg Multiplet Spectrum and Its Computer Simulation

To assess how well the two zone model describes the emission spectrum from typical resonance lamps, a number of high resolution spectra were recorded. Figure 2 shows examples of emission in the neighborhood of 253.7 nm for three different lamp conditions. Frame C is the unreversed spectrum of an optically thin lamp. It shows the 10 isotopic and hyperfine components of the 253.7 nm Hg multiplet resolved into five lines that exhibit overlap only as a result of natural and Doppler broadening. The instrument resolution (1.6×10^6) was capable of resolving lines that are about a Doppler width apart (0.022 cm^{-1} at 298 K). As a result five partially overlapping lines were readily resolved. The line due to the Hg(196) isotope was not observed because of its very low natural fractional abundance (0.0015). Its position is in the vacancy in what appears to be an otherwise equispaced ($0.15 \pm .02 \text{ cm}^{-1}$) spectrum. The spectra shown in figure 2 were not corrected for plate response non-linearities. The exposures however did not depart very much from the linear regime so that the recorded peak heights are a good approxi-

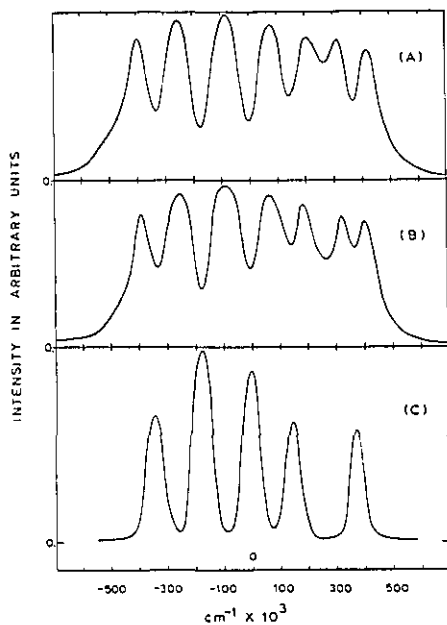


Figure 2—Frame C—A microdensitometer trace of a photographic plate showing the high resolution spectrum obtained for an optically thin, unreversed electrodeless Hg discharge lamp in the neighborhood of 253.7 nm.

Frame B—The spectrum of a reversed lamp produced by a dc discharge operated at a well regulated current of 6 mA in the same spectral region.

Frame A—The spectrum in the same spectral region of the same lamp operating at 10 mA.

mation of the relative intensities. These amplitudes are in agreement with values from the literature [8] and hence were used with some confidence in the computer program.

The high optical density lamp, operated with currents of 6 and 8 mA (frames B and A in fig. 2), shows marked self-reversal that becomes greater as the current increases and raises the lamp temperature and Hg pressure. The intensities adjacent to each of the multiplet lines changes the five line unreversed spectrum into a complex six line structure whose two outermost lines are the self-reversed wings of the two extreme lines of the unreversed quintuplet. It is clear that less of the resonance radiation emitted by the reversed lamp is absorbed by Hg vapor because of lower emission at the actual multiplet line positions. When absorption is used to determine temperature changes over a wide range, a reversed resonance lamp is the preferred choice since saturation (approach to 100% absorption) occurs with an unreversed lamp even when the optical density in the absorption cell is small.

Figure 3 shows how well a computer-simulated emission from a two zone lamp model can be made to fit an experimental spectrum. Lamp conditions and model parameters are given in the figure caption and the experimental spectrum was corrected for nonlinear plate response. Except for a difference in scale, the experimental and computed spectra are seen to be very similar with regard to line spacing and overall width. The differences in line intensities are worth noting because any further incremental changes in the model parameters did not significantly improve the agreement. The simulated spectrum shows less change in the relative peak heights and more variation at the minima than does the experimental spectrum. The reason for this undoubtedly resides in the inability of the two zone model to accurately represent the actual distribution of emitters and absorbers in the lamp.

In order to obtain an optimum match between the computer simulation and the experimental lamp emission, four parameters are required to initialize the two zone model. They are A_1 and A_2 , the ratio of Lorentz to Doppler widths in zones 1 and 2; OD_1 , the optical depth in zone 1; and R , the ratio of optical depths in zone 1 to zone 2. The quantity A_3 , the ratio of Lorentz to Doppler widths in the absorbing region 3, has been determined previously for Hg broadened by Ar [8]. It is proportional to the argon pressure and is equal to 1.0 at a pressure of about 140 torr. Since the argon pressure in the lamp was close to this pressure, A_1 and A_2 were assumed to be unity for all experimental lamp conditions. The quantities OD_1 and R on the other

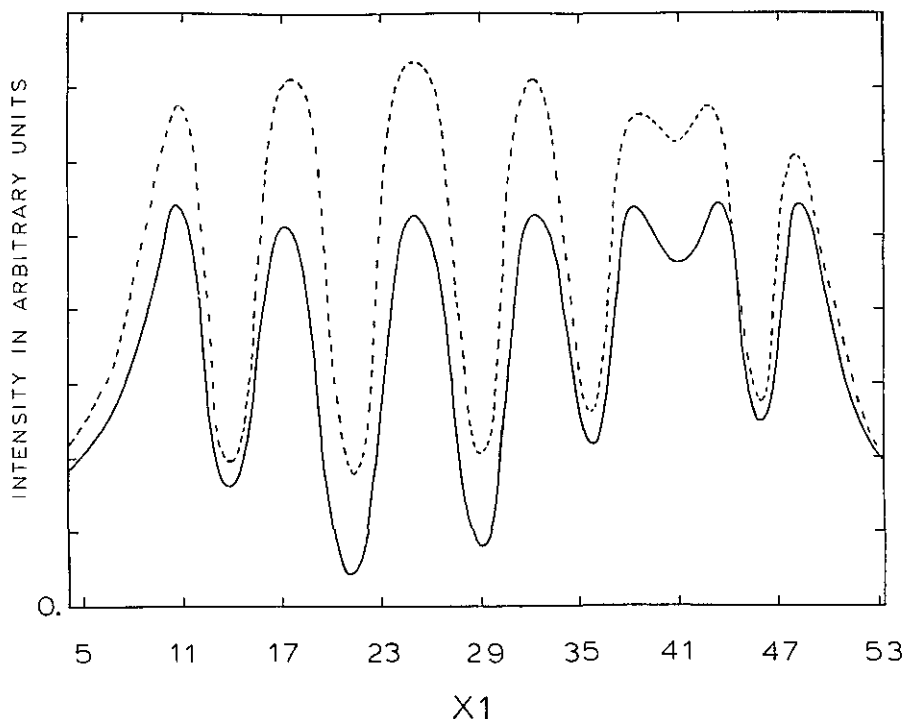


Figure 3—A microdensitometer trace that has been corrected for plate nonlinearities (dashed curve), of the high resolution spectrum emitted by the reversed Hg lamp operated at 9 mA. This is to be compared with the calculated lamp profile (solid curve) using the following lamp parameters: $A_1=A_2=1$; $OD_1=60$ and $R=3$.

hand, increase as the lamp current or temperature does because the Hg concentration and its gradient near the lamp walls are determined by these parameters.

3.2 Absorption Measurements and Their Computer Simulation

A detailed comparison of the calculated and measured integrated absorption by Hg vapor as a function of temperature and buffer gas pressure is of interest. While the computer simulated lamp emission profiles do not quite match the observed ones, it will be seen that the optimized model parameters so obtained, can be used to compute the temperature and pressure dependence of the absorption of 253.7 nm radiation quite well.

As mentioned above, the ratio of Lorentz to Doppler widths (A 's) for the $6^1S_0-6^3P_1$ Hg transition is unity when about 140 torr of argon is present as a buffer gas. Figure 4 shows experimental points plotted on a graph of fraction absorbed vs. A_3 and Argon pressure for four different lamp currents of 8, 10, 15 and 20 mA. The solid curves were calculated by means of the two zone lamp model. As discussed earlier the quantities A_1 and A_2 were assigned the constant value of one while OD_1 and R , representing emitter and absorber concentrations and their gradients, were increased as the lamp current was made larger. The values of

OD_1 and R were identical to those required to produce the best agreement with the experimental profile in figure 3. It should be noted that this computer simulation of the pressure growth curves is quantitatively better than that obtained for the lamp emission spectra.

Hg absorption data were obtained over a range of temperatures (300–900 K) by means of an electrically heated copper furnace that housed a Hg containing absorption cell. The heated portion of the cell was an evacuated fused silica cylinder that was connected to a small tube outside of the furnace. This tube (<2% of the total volume) contained a small pool of liquid mercury thermostated at 298 K. The heated absorption cell therefore contained 1.8 mTorr of Hg vapor at all furnace temperatures with a number density of Hg atoms that was inversely proportional to the furnace temperature. The 253.7 nm radiation (supplied by a reversed lamp operated at 9 mA) traversed the cylindrical absorption cell perpendicular to its axis, and was measured by the 1P28 photomultiplier-monochromator system. Curve 1 in figure 5 was calculated from an appropriate set of model parameters obtained earlier and is seen to agree well with the experimental data points. Curve 2 was calculated for a gas heated at constant volume of Hg atom number density. Figure 6 shows a set of temperature calibration curves that were calculated for the same set of lamp parameters used in figure 4. These

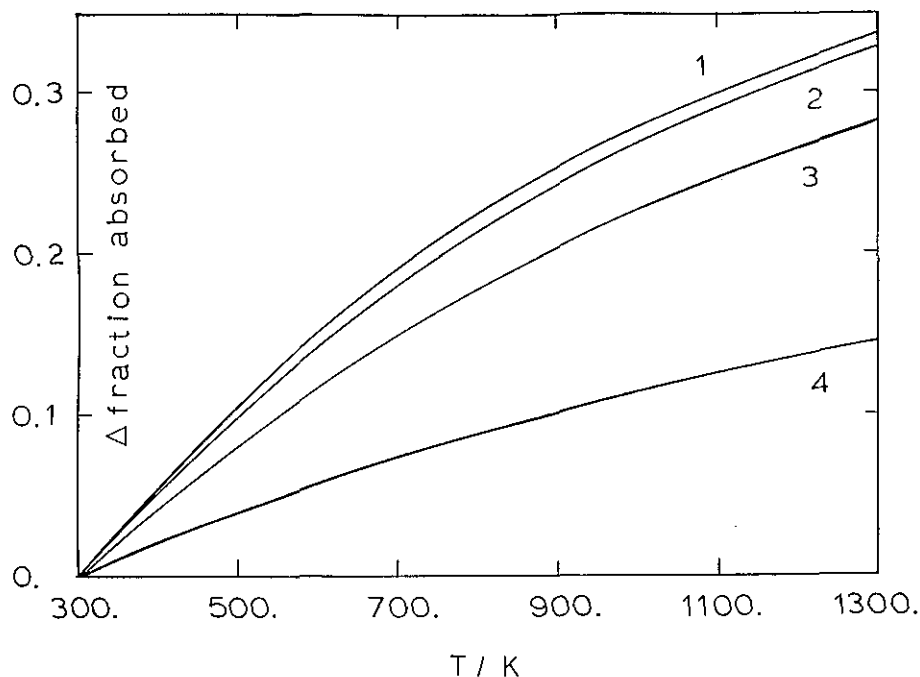


Figure 6—Computed fraction absorbed vs. temperature curves for a Hg absorption cell containing 1.8 mTorr of Hg vapor and using the same lamp parameters as those given in figure 4.

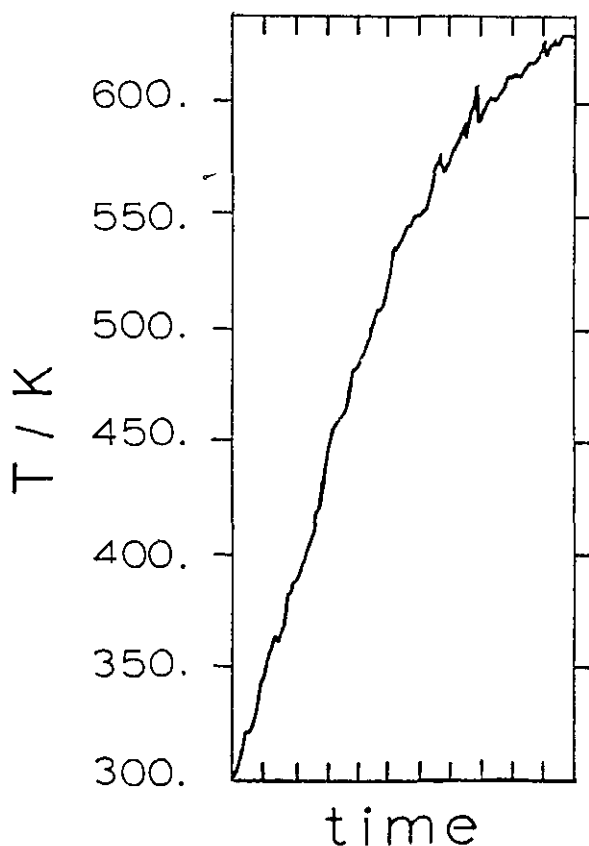


Figure 7—An experimental temperature-time curve for one Torr of a transiently heated 50:1 mixture of SF₆ and Hg vapor.
T_{eq} = 836 K, 0.8 μs/time div., 400 sweeps averaged.

curves cover a wide range of lamp optical densities and provide a basis for transient temperature measurement over large dynamic ranges.

3.3 Temperature Modulation Experiments

A typical case of constant volume heating is illustrated in figure 7 which shows a typical signal averaged curve for the temporal dependence of absorption of 253.7 nm radiation by 1.8 mTorr of Hg vapor mixed with 1 Torr of SF₆. At t=0, a 500 ns, 1 Joule pulse of 10.6 μm radiation from a CO₂ laser was absorbed by a 5 cm path through 3 cm³ of the SF₆-Hg mixture. About 25 μs after the laser pulse the vibrational excitation of the irradiated SF₆ becomes equipartitioned with its rotational and translational degrees of freedom. As the average translational energy of the SF₆ increased and the Hg atoms responded to this change, absorption of the 253.7 nm multiplet was broadened and became larger. The temperature scale shown in figure 7 was obtained from the parameters used to compute the temperature calibration curves in figure 5 and 6.

4. Conclusions

It is well known that the absorption of resonance radiation by an atomic gas is both pressure and temperature dependent because of the line broadening brought about by molecular collisions and

the Doppler effect. In particular, it has been shown here that the amount of resonance radiation absorbed in the neighborhood of 253.7 nm by a trace of Hg vapor is a measure of its translational temperature. When admixed with a gas such as SF₆, the Hg atoms can monitor the temperature changes that occur in the combined system after a 10.6 μm pulse from a CO₂ TEA laser is absorbed by the SF₆.

The multiplet emission in the neighborhood of 253.7 nm by a high optical density Hg light source was simulated by a simple two zone model. The natural line widths were enhanced by Doppler and

Lorentz broadening. Two fixed and two adjustable parameters were required to describe a wide variety of lamp conditions. It was shown that the same lamp parameters that optimized the fit of the light source emission spectra could also be used to calculate the total integrated absorption as a function of both pressure and temperature. The agreement obtained between the simulation and the experimental pressure and temperature data shows that computer derived temperature calibration curves for different lamp conditions are a reasonable basis for making transient temperature measurements in rapidly heated gases.

APPENDIX

The following describes the line shape and absorption calculations discussed above. The reader is referred to Mitchell and Zemansky for further details [1].

We designate $k(\nu_r)$ as the Napierian absorption coefficient for an isolated Doppler line which is broadened by pressure (Lorentz broadening). This quantity is the contribution of the entire Doppler line at wavelength $\nu = \nu_r$, as convoluted by a Lorentzian function and is given by the following expression:

$$\text{I. } k(\nu_r) = k(\nu_0) \int_{-\infty}^{+\infty} \frac{e^{-\left[\frac{\nu - \nu_0}{\delta}\right]^2}}{1 + \left[\frac{\nu - \nu_r}{\Delta}\right]^2} d\nu$$

where ν_r is some chosen reference frequency and ν_0 is the frequency at the center of the doppler line. The quantity δ is the Doppler half width (half line width at maximum/e) and Δ is the Lorentz half width (half line width at maximum/2) and $k(\nu_0)$ is the Napierian absorption coefficient at the line center.

In the following calculations we work with dimensionless units by making the following substitutions:

Set $X = (\nu - \nu_0)/\delta$; $X_r = (\nu_r - \nu_0)/\delta$; $Y = (\nu - \nu_0)/\Delta$;

$$Y_r = (\nu_r - \nu_0)/\Delta; \quad A = \Delta/\delta$$

Thus: $X = AY$ and $X_r = AY_r$,

The integral over the Doppler line function is

$$\int_{-\infty}^{+\infty} \exp(-X^2) \delta dX = \delta \sqrt{\pi}$$

and the integral over the Lorentz line function is given by

$$\int_{-\infty}^{+\infty} dX / (1 + ((X - X_r)/A)^2) = A \pi$$

With these integrals and definitions in mind we can express $k(\nu_r)$ in dimensionless form as follows:

$$\text{II. } k(X_r) = \frac{k'(0)}{\delta \sqrt{\pi} A \pi} \int_{-\infty}^{+\infty} \frac{e^{-X^2} dX}{1 + ((X - X_r)/A)^2}$$

where it is understood that an isolated resonance line is centered about $X=0$ and the optical depth, OD , for a pure Doppler broadened line is:

$$\text{III. } OD = \frac{k'(0)}{\delta \sqrt{\pi}} = n \cdot \sigma(0) \cdot \Lambda$$

The value of $\sigma(0)$ is the absorption cross section of the pure Doppler line at its center in units of cm², n is the molecular number density in cm⁻³ and Λ is the absorption length in cm. The quantity $\sigma(0)$ is obtained from the relation:

$$\text{IV. } \sigma(0) = \frac{\pi e^2 f}{\sqrt{\pi} \cdot mc \delta} = \frac{0.50 \cdot 10^{-12} \cdot f}{\delta}$$

where f is the oscillator strength and δ , the Doppler width, is in units of cm^{-1} and is given by:

$$\delta = \omega_0 \cdot 4.3 \cdot 10^{-7} \sqrt{T/M},$$

with ω_0 in cm^{-1} , T in K and M is the molecular weight in g/mole .

Equation II above refers to a single emission line. For j lines the following equation applies:

$$V. \quad k(X_r) = \frac{1}{A\pi} \int_{-\infty}^{+\infty} \sum_{i=1}^j \frac{OD(i) e^{-(X-L(i))^2}}{1+((X-X_r)/A)^2} dX$$

where $L(i)$ is the relative line position of the i^{th} line expressed in terms of the reduced frequency, X given above.

For each zone m in the simple model discussed in the text, the absorption coefficient $k_m(\nu_r)$ can be calculated from equation V. In each zone, the quantities X , X_2 and $L(i)$'s must be expressed on an appropriate scale of reduced frequencies. Thus X takes on values X_1 , X_r , and X_3 which are related by $X_1\delta_1 = X_2\delta_2 = X_3\delta_3$. The same applies to the X_r 's and the $L(i)$'s. Also each zone has its own value of A , namely A_1 , A_2 or A_3 .

The $OD(\text{total})$ for each zone is calculated from its temperature T_m , length and the f value for the entire transition. The $OD(i)$'s for each zone must satisfy, $OD(\text{total}) = \sum OD(i)$ and the f value for the entire transition is calculated from its lifetime: $\tau \sim 1.1 \times 10^{-7} \text{s}$, $f = 0.027$.

There are seven stable isotopes; five even and two with odd mass numbers. The latter are Hg(199) and Hg(201) with nuclear spins of 1/2 and 3/2 respectively that couple with the electron J value. The 253.7 nm multiplet is composed therefore of 10 lines: one from each of the five even mass isotopes, two from Hg(199) and three from Hg(201). The natural abundance of the Hg(196) isotope is so small that its emission is of no consequence. The five resolved lines thus consisted of the following components: [9] (frame C in fig. 2)

$\Delta\lambda/10^3\text{cm}^{-1}$	Hg isotopes	Relative Intensities
-340	204, 199a, 201a	0.64
-180	202	1.00
0	200	0.78
150	198, 201b	0.49
385	199b, 201c	0.46

Thus the f values used in the lamp simulation calculations for each of the resolved lines are:

$$f_i = (0.027) \left[\frac{I_i}{\sum I_i} \right] \quad \text{where } i = 1, 2, \dots, 5$$

and I_i is the relative intensity of the i^{th} resolved multiplet line.

References

- [1] Mitchell, A. C. G., and M. W. Zemansky, Resonance Radiation and Excited States: Cambridge University Press, 1934.
- [2] (a) Braun, W., and T. Carrington, J. Quant. Spectrosc. Radiative Transfer, **9**, 1133 (1969); (b) Braun, W., and T. Carrington, Natl. Bur. Stand. (U.S.) Tech. Note 476 (U.S. Government Printing Office, Washington, DC, 1969).
- [3] For models containing arbitrary distributions of absorbing and emitting atoms see for example: Cowan, R. D., and G. H. Dieke, Rev. Mod. Phys. **20**, 418 (1948); Tako, T., J. Phys. Soc. (Japan), **16**, 2016 (1961) and references cited therein.
- [4] (a) Michael, J. V., and R. E. Weston, Jr., J. Chem. Phys. **45**, 3632 (1966); (b) Barker, J. R., and J. V. Michael, J. Opt. Soc. Am. **58**, 1615 (1968); (c) Morse, F. A., and F. Kaufman, J. Chem. Phys. **42**, 1785 (1965); (d) Kurylo, M. J.; Peterson N. C. and W. Braun, J. Chem. Phys. **53**, 2776 (1970); (e) Davis, D. D.; R. E. Huie, J. T. Herron, M. J. Kurylo, and W. Braun, J. Chem. Phys. **56**, 4868 (1972); (f) Parkes, D. A.; L. F. Keyser and F. Kaufman, Astrophys. J. **149**, 217 (1967).
- [5] Maki, R. G.; J. V. Michael and J. W. Sutherland, J. Phys. Chem. **89**, 4815 (1985).
- [6] Braun, W.; A. M. Bass and D. D. Davis, J. Opt. Soc. Am. **60**, 166 (1970).
- [7] Lifshitz, A.; G. B. Skinner and D. R. Wood, J. Chem. Phys. **70**, 5607 (1979).
- [8] E. L. Lewis, Physics Reports **58**, 1 (1980).
- [9] Gunning, H. E., and O. P. Strausz, Adv. In Photochemistry **1**, 209 (1963).

Absolute Isotopic Abundance Ratio And Atomic Weight Of a Reference Sample of Gallium

Volume 91

Number 6

November–December 1986

L. A. Machlan, J. W. Gramlich,
L. J. Powell, and G. M. Lambert

National Bureau of Standards
Gaithersburg, MD 20899

An absolute value has been obtained for the isotopic abundance ratio of a reference sample of gallium (Standard Reference Material 994), using thermal ionization mass spectrometry. Samples of known isotopic composition, prepared from nearly isotopically pure separated gallium isotopes, were used to calibrate the mass spectrometers. The resulting absolute $^{69}\text{Ga}/^{71}\text{Ga}$ ratio is 1.50676 ± 0.00039 , which yields atom percents of $^{69}\text{Ga} = 60.1079 \pm 0.0062$ and $^{71}\text{Ga} = 39.8921 \pm 0.0062$. The atomic weight calculated from this isotopic

composition is 69.72307 ± 0.00013 . The indicated uncertainties are overall limits of error based on two standard deviations of the mean and allowances for the effects of known sources of possible systematic error.

Key words: absolute ratio; assay; atomic weight; gallium; isotopic abundance; mass spectrometry; tetraphenylarsonium chloride.

Accepted: June 25, 1986

1. Introduction

The Inorganic Analytical Research Division of the National Bureau of Standards has been conducting a long-term program of absolute isotopic abundance ratio and atomic weight determinations using high precision isotope ratio mass spectrometry. Previous atomic weight determinations include silver [1,2]¹, chlorine [3], copper [4], bromine [5], chromium [6], magnesium [7], lead [8], boron [9], rubidium [10], rhenium [11], silicon [12], potassium [13], thallium [14], and strontium [15]. The present work extends the study to gallium.

To obtain absolute isotopic ratios from the observed or relative measurements made on a mass spectrometer, it is necessary to calibrate the instru-

ment using samples of accurately known isotopic ratios of the element under study. These synthetic isotopic standards, assayed and gravimetrically prepared from chemically pure and nearly isotopically pure isotopes, provide a bias correction (calculated isotopic ratio/observed isotopic ratio) which, when applied to the observed isotopic ratio of the reference sample being calibrated, allows an absolute ratio to be calculated for the sample. The atomic weight is then obtained by multiplying the fractional abundance of each isotope by its nuclidic mass [16] and summing the resultant products. A more detailed description of the method used for the determination of isotopic abundance ratios and atomic weights at NBS is given elsewhere [2].

In 1961, the IUPAC Commission on Atomic Weights recommended a value of 69.72 for the atomic weight of gallium, based on chemical determinations by Richards and Craig [17] and Lundell and Hoffman [18], as well as isotopic measurements by Inghram et al. [19]. Two more recent determi-

About the Authors: L. A. Machlan, J. W. Gramlich, L. J. Powell, and G. M. Lambert are with the Center for Analytical Chemistry in NBS' National Measurement Laboratory.

¹ Figures in brackets indicate literature references.

nations, by coulometric assay of gallium and arsenic [20] and by calibrated isotope ratio mass spectrometry [21], have yielded values of 69.737 and 69.724, respectively. The currently recommended value [22] for the atomic weight of gallium is 69.723 ± 0.004 based on the more recent mass spectrometric measurement [21].

Isotopic fractionation of gallium by more than 10 percent has been reported when a continuous electrical current is passed through a capillary column of liquid gallium [23,24]. Recent work in this laboratory has demonstrated that gallium isotopic fractionation approaching 1 percent is possible with ion exchange chromatography [25]. A survey of commercial high-purity gallium shows a range of approximately 0.25 percent in the $^{69}\text{Ga}/^{71}\text{Ga}$ ratio for the samples investigated [26]. The origin of these variations in commercial high-purity gallium is likely the result of isotopic fractionation during the multiple recrystallization steps used for purification. Little information is available in the literature regarding isotopic variations of gallium in nature. Values reported during the past 35 years for the isotopic composition of gallium range over 3 percent; however this spread is probably due to measurement imprecision. DeLaeter [27] reports a maximum deviation of 0.11 percent in six meteorites relative to the isotopic composition of his terrestrial standard.

A relatively large discrepancy between the two recently published values for the atomic weight of gallium, combined with evidence for isotopic variations among commercial materials, provided impetus for the certification of a Standard Reference Material (SRM 994) of known isotopic composition and atomic weight.

2. Experimental Procedure²

2.1 Mass Spectrometry

Isotope ratio measurements were made on two NBS designed thermal ionization mass spectrometers equipped with 30 cm radius of curvature, 90° magnetic sectors. Each instrument contained a thin lens "Z" focussing ion source and a deep bucket Faraday cage collector [28,29]. One collector (Inst. #5) was equipped with a 50 percent transmission grid shadowing a series of suppression grids, while the other collector (Inst. #1) was of a new design, eliminating the pre-slit transmission and suppres-

sion grids but containing a double slit collimator before the Faraday cage. The remainder of the measurement circuitry consisted of a vibrating reed electrometer, precision voltmeter, and computer. Timing, magnetic field switching, and data acquisition were controlled by computer.

Gallium was thermally ionized from a tungsten filament fabricated from 0.001 in \times 0.030 in (0.0025 cm \times 0.076 cm) high purity tungsten ribbon. After fabrication, the filaments were degassed for 45 min by passing a current of 4.5 A through them in a vacuum. Filaments cleaned in this manner generally exhibited no detectable gallium signal or isobaric interferences in the gallium spectral region. Occasionally, analyses have shown small interfering peaks (presumably hydrocarbons) which can be resolved from the ^{69}Ga and ^{71}Ga mass positions. Even if not resolved, their contribution to an error in the ratio measurement of natural gallium would be less than 1 part in 10^5 . Possible isobaric interferences could produce a significant systematic bias in the measurement of the isotopic composition of the separated isotopes. This possible systematic error has been incorporated into the statistical evaluation of the experimental data and will be discussed in more detail in section 2.5 of this paper.

All sample loading was conducted in a Class 100 clean air hood. Pipets made from fused silica tubing were used to transfer the samples from their containers to the filaments. The tubing was cleaned by heating in 8M HNO_3 for 48 hours, followed by several rinsings with ultra-high purity water. Approximately 5 μL of the sample solution (500 ng Ga) was placed on the tungsten filament and dried by passing a current of 1 A through the filament for 10 min followed by a current of 3 A for 5 min. Drying was aided by a heat lamp placed 20 cm above the filament. Because the rate and degree of isotopic fractionation during the mass spectrometric analysis may be affected by variations in the sample loading procedure, all samples were loaded on a programmable sample dryer [30] which automatically and reproducibly controls the timing and currents to the filament during the sample drying procedure. After the initial drying, the filaments were transferred to a separate Class 100 clean air hood and heated for 15 s at 900 °C, using an optical pyrometer for temperature adjustment (temperature not corrected for emissivity). This final step was to ensure conversion of the sample to the most stable crystalline form of gallium oxide, $\beta\text{-Ga}_2\text{O}_3$ [31]. During this high temperature drying step, the air flow through the hood was turned off so that reproducible temperature settings could be obtained.

² Certain commercial equipment, instruments, or materials are identified in this paper to specify adequately the experimental procedure. Such identification does not imply recommendation or endorsement by the National Bureau of Standards, nor does it imply that the materials or equipment identified are necessarily the best available for the purpose.

Gallium ion currents were measured with a constant accelerating potential of 9.8 kV. The ions of each isotope were brought into alignment with the collector slit by computer controlled stepping of the magnetic field. The filament current was initially set at 2.15 A, corresponding to an optical pyrometer temperature reading of approximately 700 °C. Initially no gallium signal was observed; however, after 2–3 min, the Ga^+ would rapidly increase, reaching a total Ga^+ ion current at the collector of approximately 2×10^{-11} A at 5 min into the analysis. The filament current was adjusted at 5, 10, and 15 min into the analysis to produce gallium ion currents of 2×10^{-11} A, 4×10^{-11} A, and 6×10^{-11} A,³ and baseline measurements were taken on each side of both isotopes. Data were collected between 20 and 50 min into the analysis. Ten 1-second integrations of the ion current were made for each isotope before magnetic field switching, with an 8 s time delay between isotopes to allow for magnetic field stabilization and settling of RC time constants in the measurement circuitry.

2.2 Purification of Separated Gallium Isotopes

Electromagnetically separated ^{69}Ga and ^{71}Ga isotopes in the form of gallium oxide were obtained from the Nuclear Division, Oak Ridge National Laboratory. The ^{69}Ga was designated sample 121201 and the ^{71}Ga was designated sample 121301. The certificate which accompanied each sample showed enrichment to approximately 99.8 percent for the major isotope. The certificates included a semi-quantitative spectrographic analysis which showed that the principal impurities were sodium, magnesium, and zirconium at the 0.1 percent level or higher; and calcium, iron, potassium, lithium, rubidium, and silicon at the 0.01 to 0.05 percent level. While only the element iron was at a level where it would interfere with the assay method for gallium, several other elements, which were reported as less than 0.05 percent, could interfere if they were, in fact, near that level. Among these elements were chromium, copper, molybdenum, lead, tin, cadmium, and platinum, which could interfere with the gallium assay procedure by forming insoluble compounds with tetraphenylarsonium chloride [32].

To reduce these impurities to a level low enough so that they would not cause a significant error in the assay procedure, the separated isotopes were purified by a combination of chloride precipitation to remove insoluble chlorides, anion exchange chromatography in the thiosulfate form to reduce

the iron concentration, and then, sequentially, cation exchange and anion exchange chromatography to remove other potentially interfering impurities.

Each separated isotope was treated as follows: The gallium oxide (about 1.2 g of $^{69}\text{Ga}_2\text{O}_3$ and 0.9 g of $^{71}\text{Ga}_2\text{O}_3$) was dissolved in 100 mL of HCl (1+3).⁴ The resulting solution was evaporated to constant volume at about 50 °C. The residue was dissolved in 20 g of H_2O and filtered through fine textured filter paper. The filtrate was evaporated to 50 g and then 10 g of 0.5M HCl and 4.5 g of 0.2M KSCN were added. This solution was passed through an anion exchange column (6.4×0.8 cm filled with 2 mL of AG1×8, 100–200 mesh anion exchange resin and then cleaned and prepared with 20 g of 5M HCl, 30 g of H_2O and 20 g of a solution of 0.1M in KSCN and 0.05M in HCl) and eluted with 120 g of the solution 0.1M in KSCN and 0.05M in HCl.

The gallium solution was passed through a cation exchange column (20.5×1.6 cm filled to 15.0 cm with AG50×8, 100–200 mesh cation exchange resin cleaned and prepared with 190 g of 4M HCl and 50 g H_2O), washed with 20 g H_2O , and impurities eluted with 300 g of 0.4M HCl. The gallium was then eluted with 100 g of 4M HCl. This solution was evaporated to about 10 mL and, after cooling and the addition of 30 g of 5M HCl, it was passed through an anion exchange column (20.5×1.6 cm filled to 16 cm with AG1×8, 100–200 mesh anion exchange resin and cleaned with 40 g of 5M HCl, 190 g of 0.5M HCl, 40 g of H_2O , and 20 g of 5M HCl). Impurities were eluted with 150 g of 5M HCl and 50 g of 4M HCl. The gallium was eluted with 165 g of 0.5M HCl.

2.3 Preparation and Analysis of Separated Isotope Solutions

The purified ^{69}Ga and ^{71}Ga were transferred to 500 mL fused silica flasks and diluted to about 450 g with 0.5M HCl. The neck of each flask had been tooled to fit a No. 0 polyethylene stopper.

A preliminary assay of the gallium concentration of each separated isotope solution was accomplished by isotope dilution mass spectrometry. Two weighed portions (1.5–2 g) of each separated isotope solution were spiked with known amounts of natural gallium. After mixing, evaporation, con-

³ Ion currents are reported for Instrument #1.

⁴ A reagent dilution of (1+3) indicates 1 volume of concentrated reagent diluted with 3 volumes of pure water. If no dilution is specified, use of the concentrated reagent is implied. The acids and water used for these dilutions were produced at NBS by sub-boiling distillation [33].

version to the nitrate form, and dilution to 100 μg Ga/g solution with HNO_3 (1+9); the $^{69}\text{Ga}/^{71}\text{Ga}$ ratio was determined by thermal ionization mass spectrometry. The concentration of gallium was then calculated for each solution and used to determine the amount of each separated isotope solution required for the calibration mixes.

The solution of ^{69}Ga was designated "Ga-69" and the solution of ^{71}Ga was designated "Ga-71." Samples of the two solutions were analyzed for impurity elements by isotope dilution spark source mass spectrometry (IDSSMS) [33]. Samples equivalent to about 22 mg of Ga were spiked with 1.6×10^{-6} g of ^{109}Ag , ^{137}Ba , ^{111}Cd , ^{53}Cr , ^{65}Cu , ^{54}Fe , ^{41}K , ^{26}Mg , ^{97}Mo , ^{145}Nd , ^{206}Pb , ^{110}Pd , ^{195}Pt , ^{185}Re , ^{82}Se , ^{117}Sn , ^{86}Sr , ^{125}Te , ^{203}Tl , ^{91}Zr . The solutions were evaporated to dryness, a few drops of HNO_3 were added, and the solutions were again evaporated to dryness. The HNO_3 addition and the evaporations were repeated two more times. Table 1 shows the results of these analyses as well as the results of the analysis of a doped natural gallium sample which was purified in the same manner as the separated isotopes. This sample had been doped with 0.1 percent of Ba, Cd, Cr, Cu, Fe, K, Mo, Pb, Pt, Re, Se, Sn, Sr, Te, and Tl to determine the efficiency of the purification procedure.

The only element that was detected at a concentration level high enough to interfere with the assay of gallium was iron in both separated isotopes.

This apparently came from inefficiency in the purification of the separated isotopes during the separation of gallium from iron on the ion exchange column using thiocyanate, or from a higher level of iron in the two separated isotopes than reported in the spectrographic analysis that accompanied them, since the iron in the doped gallium sample was reduced by more than an order of magnitude in the purification procedure. Iron does interfere in the assay procedure but did not affect the mass spectrometric ratio measurement on test samples. Therefore it was decided to correct for iron in the assay rather than try further purification. To determine how much iron precipitated with the gallium in the tetraphenylarsonium precipitation, the material was analyzed for iron by IDSSMS. After the assay an amount equal to about 5 mg of gallium was taken from each of the precipitates and spiked with ^{57}Fe . The spiked samples were dissolved in H_2O and a few drops of HCl , and evaporated to dryness. The residue was dissolved in 5 g of H_2O and passed through a cation exchange column (6.3×0.9 cm filled to 3 cm with AG 50 \times 8, 100–200 mesh cation exchange resin and pre-cleaned with 45 g of 3M HCl and 25 g H_2O). After elution with 30 g of 0.75M HCl , the gallium and iron were removed with 10 g of 3M HCl . This solution was evaporated to dryness, a few drops of HNO_3 were added, and the solution was again evaporated to dryness. The HNO_3 addition and the evaporation were repeated and the sample was analyzed by spark source mass spectrometry. The correction for the iron was found to be 0.176 μg of $(\text{C}_6\text{H}_5)_4\text{AsFeCl}_4$ per mg of $(\text{C}_6\text{H}_5)_4\text{As}^{69}\text{GaCl}_4$ and 0.658 μg of $(\text{C}_6\text{H}_5)_4\text{AsFeCl}_4$ per mg of $(\text{C}_6\text{H}_5)_4\text{As}^{71}\text{GaCl}_4$. This correction was applied to the weights of the precipitates in the assay of "Ga-69" and "Ga-71."

Table 1. Analysis of impurities in gallium separated isotopes.

Element	Spike Isotope	Ga		
		Doped and Purified	^{69}Ga ($\mu\text{g}/\text{g}$)	^{71}Ga ($\mu\text{g}/\text{g}$)
Ag	^{109}Ag	10	6	14
Ba	^{137}Ba	10	-- ^a	7
Cd	^{111}Cd	1	nd ^b	nd
Cr	^{53}Cr	4	1.7	1.2
Cu	^{65}Cu	9	8	7
Fe	^{54}Fe	94	83	434
K	^{41}K	10	9	5
Mg	^{26}Mg	2	36	5
Mo	^{97}Mo	<1	nd	<1
Nd	^{145}Nd	3	<1	<1
Pb	^{206}Pb	2	5	4
Pd	^{110}Pd	14	<2	11
Pt	^{195}Pt	<1	nd	nd
Re	^{185}Re	—	1	nd
Se	^{82}Se	<1	nd	<1
Sn	^{117}Sn	<1	6	6
Sr	^{86}Sr	1	2	18
Te	^{125}Te	<1	<1	<1
Tl	^{203}Tl	1	1	1
Zr	^{91}Zr	<1	<1	1

^a Interference

^b Not detected

2.4 Assay of Separated Isotope Solutions

Four weighed portions containing approximately 0.75 mmol of gallium were withdrawn from each separated isotope solution in the following manner. A No. 0 polyethylene stopper with a 20 cm Teflon needle inserted through it was used to replace the stopper in the flask. A 20 mL all-polypropylene/polyethylene syringe was attached to the hub of the needle and the desired amount of solution was withdrawn. The syringe was then disconnected from the hub and the tip was capped with a plastic cap. Any static charge that might be present on the plastic syringe was dissipated by wiping it with a damp lintless towel and placing it on the balance pan which was surrounded by sev-

eral polonium anti-static sources. The syringe and contents were weighed on a semimicro balance to ± 0.02 mg. The solution was then delivered from the syringe into a 100 mL Teflon-FEP beaker and the syringe was again capped, wiped, and weighed. The weight of the sample was determined from the weights of the syringe before and after the delivery of the sample. Two assay samples were withdrawn from each solution before the calibration samples were withdrawn, and two assay samples were withdrawn after the calibration samples to ensure that no change in concentration occurred during the time interval (about 4 hours) required for the aliquoting.

Each weighed sample was assayed as follows: The sample was evaporated to constant volume at low heat (~ 50 °C) and after cooling to room temperature, 20 g of 6M HCl and 10 g of sub-boiling distilled acetone were added. A weighed portion of tetraphenylarsonium chloride $[(C_6H_5)_4AsCl \cdot 2H_2O]$ reagent solution (prepared by dissolving tetraphenylarsonium chloride hydrochloride in water, filtering, and diluting with water to 50 mg tetraphenylarsonium chloride hydrochloride per gram of solution) equal to 105 percent of the amount required to form $(C_6H_5)_4AsGaCl_4$ was combined with 20 g of sub-boiling distilled acetone and added to each assay sample. The solution was mixed using a Teflon rod and covered for 2 hours to allow bubbles to form and break. The cover was rinsed with water and the acetone and some water were allowed to evaporate from the uncovered beaker in a Class-100 clean air hood until approximately 23 g of solution remained in the beaker (about 48 hours). (The $(C_6H_5)_4AsGaCl_4$ that is formed is soluble in the initial acetone-water-hydrochloric acid mixture and slowly crystallizes from the solution as the acetone evaporates, producing relatively large crystals when compared to the usual method of precipitation.)

The crystallized $(C_6H_5)_4AsGaCl_4$ was transferred with 5M HCl to a tared 15 mL Munroe crucible. Since it was not possible to transfer the salt completely, the material remaining in the beaker was dissolved with acetone and 5M HCl, and the acetone evaporated at 50 °C. As much of the salt as possible was washed into the filtering crucible using 5M HCl. The dissolution, evaporation, and transfer procedure was repeated to minimize the amount of material remaining in the beaker. The material in the crucible was washed three times with 5M HCl (a total of 30–35 g of 5M HCl was used for transfer and washing). The crucible and contents were dried at 10 °C for 16 hours. (The filtrate was transferred back to the original beaker

and reserved for the determination of dissolved and untransferred gallium.)

The filtering crucible and contents were cooled in a desiccator, transferred to the case of a microbalance, and allowed to stand for at least 3 hours. The crucible and contents were weighed to ± 0.002 mg. A combination blank and buoyancy correction was made by averaging three crucibles that had been used to filter blank samples that had been carried through the procedure. The drying, cooling, and weighing were repeated until constant weight was reached. The air weight of the $(C_6H_5)_4AsGaCl_4$ was then determined and converted to vacuum weight using a measured value of 1.53 as the density of the salt. The micromols of gallium present in the salt were determined using a calculated atomic weight for gallium and 1983 IUPAC standard atomic weight values for the other elements. The formula weights used were 594.0886 for $(C_6H_5)_4As^{69}GaCl_4$ and 596.0770 for $(C_6H_5)_4As^{71}GaCl_4$.

The filtrate from the precipitation of the $(C_6H_5)_4AsGaCl_4$ was diluted to approximately 120 g with H_2O and warmed to approximately 40 °C to ensure that any untransferred salt was dissolved. After stirring, cooling and thorough mixing, a weighed portion (approximately 15 g) of the filtrate solution was transferred to a 50 mL Teflon-FEP beaker. The "Ga-69" solutions were spiked with about 0.2 μmol of ^{71}Ga and the "Ga-71" solutions were spiked with about 0.2 μmol of ^{69}Ga for determining soluble and untransferred gallium by isotope dilution mass spectrometry.

The spiked solution was mixed, evaporated to dryness, and dissolved in 5 g of H_2O . This solution was passed through a cation exchange column (6.3 \times 0.9 cm filled to 3 cm with AG 50 \times 8, 100–200 mesh cation exchange resin and cleaned with 45 g of 3M HCl and 20 g H_2O), washed with a few mL of H_2O and then 25 g of 0.75M HCl. The gallium was eluted with 10 g of 3M HCl and the eluate was evaporated to dryness on a hot plate at low heat. The residue was dissolved in a few drops of HNO_3 , and the $^{69}\text{Ga}/^{71}\text{Ga}$ ratio was determined by thermal ionization mass spectrometry. The gallium found as soluble Ga was added to the amount of gallium determined by gravimetry to yield the total gallium in the sample. Table 2 shows the results of these analyses.

This method of determining the concentration of gallium solutions was previously tested on solutions containing known amounts of gallium. Solutions were prepared from high purity gallium, SRM 994. The gallium concentration in eight sets of four samples, each containing 690 to 835 μmol

Table 2. Concentration of gallium separated isotope solutions.

Solution	Sample No.	Weight GaTPA (g)	Ga From GaTPA (mmol)	Ga From Filtrate (mmol)	Total Ga (mmol)	Weight Sample (g)	Concentration (mmol Ga/g)
"Ga 69"	1	0.439984	0.740607	0.001491	0.742098	28.97604	0.0256107
	2	0.439859	0.740397	0.001350	0.741747	28.96352	0.0256097
	3	0.440873	0.742104	0.001549	0.743653	29.02848	0.0256180
	4	0.435266	0.732666	0.001275	0.733941	28.65412	0.0256138
						Average	0.0256131
"Ga 71"	1	0.488208	0.751930	0.001206	0.753136	37.17272	0.0202604
	2	0.456157	0.765265	0.001233	0.766498	37.83944	0.0202566
	3	0.465770	0.781392	0.001009	0.782401	38.61812	0.0202599
	4	0.462792	0.776396	0.001576	0.777972	38.40359	0.0202578
						Average	0.0202587

of gallium were determined as described above. Comparison of the calculated and measured concentrations detected a positive bias of about 0.06 percent, but this would have a negligible effect on the ratio of the two assays since the assay for the separated isotopes would be biased by the same 0.06 percent.

2.5 Isotopic Analysis of the Separated Isotope Solutions

Each of the separated isotope solutions were analyzed eight times on each of the instruments. The ion sources were cleaned between the analyses of the two solutions as a precaution against the possibility of cross-contamination from the source parts, however, preliminary measurements showed that the two separated isotopes could be analyzed back-to-back on the same source with no detectable cross-contamination. The precision of the $^{69}\text{Ga}/^{71}\text{Ga}$ isotopic measurements on the separated isotopes is approximately 0.25 percent, however an uncertainty of 2 percent has been assigned to the measurements to cover possible sources of systematic error [34].

As the gallium mass spectrometric procedure was being developed, small mass peaks on the high mass sides of masses 69 and 71 were occasionally observed. These small isobaric interferences are attributed to organic species and could be resolved from the ^{69}Ga and ^{71}Ga masses by careful focussing of the ion source. The maximum intensity of these interfering isobars was approximately $1 \times 10^{-15}\text{A}$. Even if not resolved from the gallium masses, the contribution to systematic errors in the measurement of the natural $^{69}\text{Ga}/^{71}\text{Ga}$ ratio would be less than 1 part in 10^5 . However, in the case of the separated isotopes, these interferences, if undetected,

could produce a systematic error in the measurement of the $^{69}\text{Ga}/^{71}\text{Ga}$ ratio of the separated isotopes of up to one percent. Thus the 2 percent uncertainty assigned to the separated isotope ratio measurements reflects random errors and the maximum (worst-case) systematic errors expected from possible isobaric interferences and the measurement system non-linearities associated with large isotopic ratios. The corrected isotopic compositions of the separated isotopes are given in table 3.

Table 3. Isotopic composition of the gallium separated isotopes.

Separated Isotopes	Isotopic Composition (atom percent)			
	Operator 1	Operator 2	Mean	
"Ga 69"	^{69}Ga	99.82120	99.82094	99.8211 + 0.0036
	^{71}Ga	0.17880	0.17906	0.1789 + 0.0036
"Ga 71"	^{69}Ga	0.20449	0.20417	0.2043 + 0.0041
	^{71}Ga	99.79551	99.79583	99.7957 + 0.0041

^a The uncertainty of the ratio determination is taken to be 2 percent, which is much larger than the 95 percent confidence limit, to take into account possible biases and non-linear instrumental behavior for ratios as large as these.

2.6 Preparation of Calibration Samples

Seven calibration samples were prepared by mixing weighed portions of the "Ga-69" and "Ga-71" solutions to produce $^{69}\text{Ga}/^{71}\text{Ga}$ ratios ranging from 0.3 to 7.5. Five of the calibration mixes were within 2 percent of the natural ratio of 1.507. The portions were withdrawn from the flasks and weighed in the manner previously described for the assay of the solutions. The portions weighed from 3.2 to 24.0 g and each was weighed to ± 0.05 mg. It is therefore estimated that the weighing error for

each mix should not exceed two parts in 10^5 . To minimize any significant possibility of change in concentration of the isotope solutions with time, the portions for the calibration mixes were withdrawn from the flasks between the samples taken for assay, over a period of about 4 hours.

Each calibration mix was thoroughly mixed, the sides of the beaker were washed with H_2O and 0.2M HCl, and evaporated to dryness at low heat ($\sim 50^\circ C$) on a hot plate. The residue was dissolved in 2 mL of 8M HNO_3 and the mix was evaporated to dryness. The addition of 8M HNO_3 and evaporation to dryness was repeated two additional times. The residue was then dissolved and diluted with HNO_3 (1+9) to 1 mg Ga per gram of solution. After thorough mixing, a portion of this solution was diluted with HNO_3 (1+9) to 100 μg Ga per g of solution and transferred to small polyethylene bottles. The isotopic compositions of the calibration mixes are given in table 4.

2.7 Isotopic Analyses of the Calibration Mixes and the Reference Sample

Two complete sets of analyses of the calibration mixes and reference sample were performed by Operator 1 on MS #1 and Operator 2 on MS #5. Each operator performed four analyses of each calibration mix and 28 analyses of the reference sample. The samples were run in a pattern alternating randomly selected mixes with the reference sample.

3. Results and Discussion

The results of the measurement of the seven calibration mixes are shown in table 5. The correction factors for each analyst varied over a range of 0.030 percent for Operator 1 and 0.017 percent for Operator 2. The major spread in the calibration mixes results from the non-point calibration mixes 1 and 7. The deviation from the five point calibration mixes is especially evident for Operator 1. Two hypotheses have been proposed to explain these results. First, if there is an error in the measured isotopic composition of the ^{69}Ga separated isotope (still within the stated uncertainty), this could bring mixes 1 and 7 into agreement with mixes 2 through 6 and would also result in improving the agreement between Operator 1 and Operator 2 on the corrected $^{69}Ga/^{71}Ga$ ratio of the reference sample. The second hypothesis involves the voltage coefficient of the 10^{11} ohm input resistor of the electrometers used in this experiment. In order to maintain a constant fractionation correction for the reference sample and the point calibration mixes, it is necessary to maintain a constant total signal intensity. Any non-linearities in the input resistor would be corrected by comparing the reference sample and the point calibration mixes since the signal intensity would be the same for both isotopes for each of these solutions. This systematic bias would thus be constant and self-correcting for the reference sample and the point calibration mixes, being included as part of the correction factor. For mixes 1 and 7,

Table 4. Isotopic composition of calibration mixes.

Solution No.	Isotope Solution	Weight Solution (g)	$^{69}Ga^a$ From Solution (mmol)	$^{71}Ga^a$ From Solution (mmol)	Total ^{69}Ga (mmol)	Total ^{71}Ga (mmol)	Ratio 69/71																																																																				
1	"Ga 69"	24.02523	0.614260	0.001101	0.614426	0.082318	7.46403																																																																				
	"Ga 71"	4.01722	0.000166	0.081217				2	"Ga 69"	7.49458	0.191616	0.000343	0.191881	0.129783	1.47848	"Ga 71"	6.40240	0.000265	0.129439	3	"Ga 69"	7.65190	0.195638	0.000351	0.195905	0.130609	1.49994	"Ga 71"	6.44291	0.000267	0.130258	4	"Ga 69"	7.67884	0.196327	0.000352	0.196597	0.132142	1.48777	"Ga 71"	6.51866	0.000270	0.131790	5	"Ga 69"	7.98143	0.204064	0.000366	0.204337	0.133765	1.52758	"Ga 71"	6.59828	0.000273	0.133399	6	"Ga 69"	7.94366	0.203098	0.000364	0.203368	0.132582	1.53391	"Ga 71"	6.53982	0.000271	0.132218	7	"Ga 69"	3.24697	0.083016	0.000149	0.083590	0.280551	0.297950
2	"Ga 69"	7.49458	0.191616	0.000343	0.191881	0.129783	1.47848																																																																				
	"Ga 71"	6.40240	0.000265	0.129439				3	"Ga 69"	7.65190	0.195638	0.000351	0.195905	0.130609	1.49994	"Ga 71"	6.44291	0.000267	0.130258	4	"Ga 69"	7.67884	0.196327	0.000352	0.196597	0.132142	1.48777	"Ga 71"	6.51866	0.000270	0.131790	5	"Ga 69"	7.98143	0.204064	0.000366	0.204337	0.133765	1.52758	"Ga 71"	6.59828	0.000273	0.133399	6	"Ga 69"	7.94366	0.203098	0.000364	0.203368	0.132582	1.53391	"Ga 71"	6.53982	0.000271	0.132218	7	"Ga 69"	3.24697	0.083016	0.000149	0.083590	0.280551	0.297950	"Ga 71"	13.86943	0.000574	.280403								
3	"Ga 69"	7.65190	0.195638	0.000351	0.195905	0.130609	1.49994																																																																				
	"Ga 71"	6.44291	0.000267	0.130258				4	"Ga 69"	7.67884	0.196327	0.000352	0.196597	0.132142	1.48777	"Ga 71"	6.51866	0.000270	0.131790	5	"Ga 69"	7.98143	0.204064	0.000366	0.204337	0.133765	1.52758	"Ga 71"	6.59828	0.000273	0.133399	6	"Ga 69"	7.94366	0.203098	0.000364	0.203368	0.132582	1.53391	"Ga 71"	6.53982	0.000271	0.132218	7	"Ga 69"	3.24697	0.083016	0.000149	0.083590	0.280551	0.297950	"Ga 71"	13.86943	0.000574	.280403																				
4	"Ga 69"	7.67884	0.196327	0.000352	0.196597	0.132142	1.48777																																																																				
	"Ga 71"	6.51866	0.000270	0.131790				5	"Ga 69"	7.98143	0.204064	0.000366	0.204337	0.133765	1.52758	"Ga 71"	6.59828	0.000273	0.133399	6	"Ga 69"	7.94366	0.203098	0.000364	0.203368	0.132582	1.53391	"Ga 71"	6.53982	0.000271	0.132218	7	"Ga 69"	3.24697	0.083016	0.000149	0.083590	0.280551	0.297950	"Ga 71"	13.86943	0.000574	.280403																																
5	"Ga 69"	7.98143	0.204064	0.000366	0.204337	0.133765	1.52758																																																																				
	"Ga 71"	6.59828	0.000273	0.133399				6	"Ga 69"	7.94366	0.203098	0.000364	0.203368	0.132582	1.53391	"Ga 71"	6.53982	0.000271	0.132218	7	"Ga 69"	3.24697	0.083016	0.000149	0.083590	0.280551	0.297950	"Ga 71"	13.86943	0.000574	.280403																																												
6	"Ga 69"	7.94366	0.203098	0.000364	0.203368	0.132582	1.53391																																																																				
	"Ga 71"	6.53982	0.000271	0.132218				7	"Ga 69"	3.24697	0.083016	0.000149	0.083590	0.280551	0.297950	"Ga 71"	13.86943	0.000574	.280403																																																								
7	"Ga 69"	3.24697	0.083016	0.000149	0.083590	0.280551	0.297950																																																																				
	"Ga 71"	13.86943	0.000574	.280403																																																																							

^a Calculated using mean value from table 3.

Table 5. Determination of correction factors.

Calibration Sample No.	Calculated	Isotopic Ratio, $^{69}\text{Ga}/^{71}\text{Ga}$		Correction Factors	
		Operator 1	Operator 2	Operator 1	Operator 2
1	7.46403	7.568871	7.572529	0.986148	0.985672
2	1.47848	1.499598	1.499846	0.985917	0.985754
3	1.49994	1.521338	1.521528	0.985932	0.985809
4	1.48777	1.509024	1.509266	0.985917	0.985759
5	1.52758	1.549398	1.549678	0.985916	0.985738
6	1.53391	1.555855	1.555955	0.985897	0.985834
7	0.297950	0.3022232	0.3022426	0.985860	0.985796
Mean Values of Calibration Factors				0.985941	0.985766

it was necessary to increase the signal intensity of the major isotope relative to the minor isotope thus introducing possible systematic bias due to non-linear response of the input resistor. An error for instrument #1 of approximately 70 parts per million per volt would correct the discrepancy between mixes 1 and 7 and the point calibrations. Preliminary measurements in this laboratory on resistors of the type used in the electrometers, indicate that non-linearities of this magnitude are not unreasonable. This effect would produce a systematic error in the measurement of the separated isotopes of approximately 0.03 percent, well within the conservative uncertainty of 2 percent placed on the measurement of the isotopes.

Table 6 summarizes the observed and corrected $^{69}\text{Ga}/^{71}\text{Ga}$ values for the reference sample for Operators 1 and 2, respectively, as well as the absolute isotopic abundance ratio for gallium and its uncertainty.

Table 6. Determination of corrected isotopic ratios of the reference material.

	Observed $^{69}\text{Ga}/^{71}\text{Ga}$	Correction Factor	Corrected $^{69}\text{Ga}/^{71}\text{Ga}$
Operator 1	1.528283	0.985941	1.506797
Operator 2	1.528488	0.985766	1.506732
		Mean	1.50676
		\pm	0.00039

Table 7 gives summary calculations for the reference sample. The atomic weight is calculated from the absolute isotopic abundance by summing the product of the nuclidic masses [16] and the corresponding atom fractions.

The reference sample is issued by the NBS Office of Standard Reference Materials as SRM 994, Gallium Metal Isotopic Standard, and is certified for isotopic composition.

Table 7. Summary calculations of the atomic weight of gallium.

(1) Values	(2) Overall Limit of Error ^a	Uncertainty Components		(5) Error in Composition of Separated Isotopes
		(3) Mass Spectrometric Analytical Error (2SD of the Mean)	(4) Limits to Error in Chemical Analysis (2SD of the Mean)	
Atomic Weight=69.72307	$\pm 0.000127^b$	± 0.000023	± 0.000065	± 0.000055
Nuclidic Masses ($^{12}\text{C}=12$)				
$^{69}\text{Ga}=68.9255809$	± 0.0000033			
$^{71}\text{Ga}=70.9247005$	± 0.0000025			
Atom Percent				
$^{69}\text{Ga}=60.1079$	± 0.0062	± 0.0011	± 0.0032	± 0.0028
$^{71}\text{Ga}=39.8921$	± 0.0062	± 0.0011	± 0.0032	± 0.0028
Isotopic Ratio				
$^{69}\text{Ga}/^{71}\text{Ga}=1.50676$	± 0.00039	± 0.000070	± 0.000204	± 0.000174

^a The overall limit of error (2) is the sum of 2 standard deviation limits for random error plus the term covering possible systematic error in the separated isotopes. The error components are combined as follows:

$$(2) = [(3)^2 + (4)^2]^{1/2} + (5)$$

Where the numbers in parentheses refer to numbers in column headers.

^b Includes a contribution of 0.000003 for uncertainty in nuclidic masses.

We are indebted to: Keith R. Eberhardt for statistical analysis of the data; William A. Bowman III and Ronald W. Shideler for instrumental maintenance support; and Paul J. Paulsen for supervision of the spark source mass spectrometric measurements of the separated isotopes.

References

- [1] Shields, W. R.; E. L. Garner and V. H. Dibeler, Absolute isotopic abundance of terrestrial silver. *J. Res. Natl. Bur. Stand. (U.S.)* **66A-1**: 1-3; 1962.
- [2] Powell, L. J.; T. J. Murphy and J. W. Gramlich, The absolute isotopic abundance and atomic weight of a reference sample of silver. *J. Res. Natl. Bur. Stand. (U.S.)* **87-1** 9-19; 1982.
- [3] Shields, W. R.; T. J. Murphy, E. L. Garner, and V. H. Dibeler, Absolute isotopic abundance ratio and the atomic weight of chlorine. *J. Amer. Chem. Soc.*, **84**: 1519-1522; 1962 May 5.
- [4] Shields, W. R.; T. J. Murphy and E. L. Garner, Absolute isotopic abundance ratio and atomic weight of copper. *J. Res. Natl. Bur. Stand. (U.S.)* **68A-6**: 589-592; 1964.
- [5] Catanzaro, E. J.; T. J. Murphy, E. L. Garner, and W. R. Shields, Absolute isotopic abundance ratio and the atomic weight of bromine. *J. Res. Natl. Bur. Stand. (U.S.)* **68A-6**: 593-599; 1964.
- [6] Shields, W. R.; T. J. Murphy, E. J. Catanzaro, and E. L. Garner, Absolute isotopic abundance ratio and the atomic weight of a reference sample of chromium. *J. Res. Natl. Bur. Stand. (U.S.)* **70A-2**: 193-197; 1966.
- [7] Catanzaro, E. J.; T. J. Murphy, E. L. Garner, and W. R. Shields, Absolute isotopic abundance ratio and atomic weight of magnesium. *J. Res. Natl. Bur. Stand. (U.S.)* **70A-6**: 453-458; 1966.
- [8] Catanzaro, E. J.; T. J. Murphy, W. R. Shields, and E. L. Garner, Absolute isotopic abundance ratios of common, equal-atom, and radiogenic lead isotope standards. *J. Res. Natl. Bur. Stand. (U.S.)* **72A-3**: 261-267; 1968.
- [9] Catanzaro, E. J.; C. E. Champion, E. L. Garner, G. Marinenko, K. M. Sappenfield, and W. R. Shields, Standard Reference Materials: Boric acid; isotopic and assay Standard Reference Materials. *Natl. Bur. Stand. (U.S.) Spec. Publ.* 260-17; 1970 February, 60 pp.
- [10] Catanzaro, E. J.; T. J. Murphy, E. L. Garner, and W. R. Shields, Absolute isotopic abundance ratio and atomic weight of terrestrial rubidium. *J. Res. Natl. Bur. Stand. (U.S.)* **73A-5**: 511-516; 1969.
- [11] Gramlich, J. W.; T. J. Murphy, E. L. Garner, and W. R. Shields, Absolute isotopic abundance ratio and atomic weight of a reference sample of rhenium. *J. Res. Natl. Bur. Stand. (U.S.)* **77A-6**: 691-698; 1973.
- [12] Barnes, I. L.; L. J. Moore, L. A. Machlan, T. J. Murphy, and W. R. Shields, Absolute isotopic abundance ratios and the atomic weight of a reference sample of silicon. *J. Res. Natl. Bur. Stand. (U.S.)* **79A-6**: 727-735; 1975.
- [13] Garner, E. L.; T. J. Murphy, J. W. Gramlich, P. J. Paulsen, and I. L. Barnes, Absolute isotopic abundance ratios and atomic weight of a reference sample of potassium. *J. Res. Natl. Bur. Stand. (U.S.)* **79A-6**: 713-725; 1975.
- [14] Dunstan, L. P.; J. W. Gramlich, I. L. Barnes, and W. C. Purdy, Absolute isotopic abundance and the atomic weight of a reference sample of thallium. *J. Res. Natl. Bur. Stand. (U.S.)* **85-1**: 1-10; 1980.
- [15] Moore, L. J.; T. J. Murphy and I. L. Barnes, Absolute isotopic abundance and atomic weight of a reference sample of strontium. *J. Res. Natl. Bur. Stand. (U.S.)* **87-1**: 1-8, 1982.
- [16] Wapstra, A. H. and G. Audi, Atomic Data and Nuclear Data Tables. *Nuclear Physics A432-1*: 1-55; 1985.
- [17] Richards, T. W., and W. M. Craig, The atomic weight of gallium. *J. Am. Chem. Soc.* **45**: 1155-1167; 1923.
- [18] Lundell, G. E. F., and J. I. Hoffman, Atomic weight of gallium. *J. Res. Natl. Bur. Stand. (U.S.)* **15**: 409-420; 1923.
- [19] Inghram, M. G.; D. C. Hess, H. S. Brown, and E. Goldberg, On the isotopic composition of meteoritic and terrestrial gallium. *Phys. Rev.* **74**: 343-344; 1948.
- [20] Marinenko, G., On the atomic weight of gallium. *J. Res. Natl. Bur. Stand. (U.S.)* **81A-1**: 1-4; 1977.
- [21] DeLaeter, J. R., and K. J. R. Rosman, The atomic weight of gallium. *Int. J. Mass Spectrom. Ion Phys.* **21**: 403-409; 1976.
- [22] Holden, N. E., and R. L. Martin, The atomic weights of the elements 1983. *Pure & Appl. Chem.* **56** (6): 653-674; 1984.
- [23] Nief, G., and E. Roth, Sur un phenomene de separation d'isotopes provoqué par passage de courant électrique dans un metal fondu. *Comp. Rend. Acad. Sci. Paris* **239**: 162; 1954.
- [24] Goldman, M.; G. Nief and E. Roth, Influence de la temperature sur la separation isotopique sous l'effet du courant dans le gallium fondu. *Hebd. Seances Acad. Sci.* **243**: 1414-1416; 1956.
- [25] Machlan, L. A., and J. W. Gramlich, Isotopic fractionation of gallium on an ion exchange column (in preparation).
- [26] Gramlich, J. W., and L. A. Machlan, Isotopic variations in commercial high-purity gallium, *Anal. Chem.* **57** (8): 1788-1790; 1985.
- [27] DeLaeter, J. R., The isotopic composition and elemental abundance of gallium in meteorites and in terrestrial samples. *Geochim. Cosmochim. Acta* **36**: 735-743; 1972.
- [28] Shields, W. R., ed. Analytical Mass Spectrometry Section: Instrumentation and procedures for isotopic analysis. *Natl. Bur. Stand. (U.S.) Tech. Note* 277; 1966 July, 99 p.
- [29] Garner, E. L.; L. A. Machlan and W. R. Shields, Standard Reference Materials: Uranium isotopic standard reference materials. *Natl. Bur. Stand. (U.S.) Spec. Publ.* 260-27; 1971 April, 150 p.
- [30] Gramlich, J. W., and R. W. Shideler, A programmable sample dryer for thermal ionization mass spectrometry. *Natl. Bur. Stand. (U.S.) Tech. Note* 1154; 1982 January, 19 p.
- [31] Roy, R.; V. G. Hill and E. F. Osborn, Polymorphism of Ga₂O₃ and the system Ga₂O₃-H₂O. *J. Am. Chem. Soc.* **74**: 719-722; 1952.
- [32] Williard, H. H., and G. M. Smith. Tetraphenylarsonium chloride as an analytical reagent. *Ind. Eng. Chem. (Anal. Ed.)* **11**: 269-274, 305-306; 1939.
- [33] Kuehner, E. C.; R. A. Alvarez, P. J. Paulsen, and T. J. Murphy, Production and analysis of high purity acids purified by sub-boiling distillation. *Anal. Chem.* **44** (12): 2050-2056; 1972 October.
- [34] Eberhardt, K. R., Statistical evaluation of uncertainties for the absolute isotopic abundance and atomic weight of a reference sample of gallium. (To be published.)

Thermal Expansion of Platinum And Platinum-Rhodium Alloys

Volume 91

Number 6

November-December 1986

R. E. Edsinger, M. L. Reilly,
and J. F. Schooley

National Bureau of Standards
Gaithersburg, MD 20899

This paper contains descriptions of the construction and use over the temperature range $-27\text{ }^{\circ}\text{C}$ to $570\text{ }^{\circ}\text{C}$ of a Merritt-Saunders (optical interferometric) linear thermal expansion apparatus. Measurements of thermal expansion are reported for platinum and for two platinum-rhodium alloys (nominally 12 wt% Rh and 20 wt% Rh). Detailed analyses are given of the measurement uncertainties involved in the experiment and of the representa-

tion of the data by polynomials in the sample temperatures. The data show precision at the 1-ppm level and good agreement with results already published.

Key words: coefficient of thermal expansion; optical interferometry; platinum; platinum-rhodium alloys; thermal expansion.

Accepted: July 23, 1986

1. Introduction

An accurate knowledge of thermal expansion is required for several different types of metrological experiments [1-3].¹ One exacting need is found in the study of thermodynamic temperature by the method of "constant-volume" gas thermometry; despite its name, this method involves a careful accounting for the unavoidable change of the volume of the gas bulb with temperature, leading to a correction of measured pressure ratios by as much as several percent.

Careful measurements have been made on the thermal expansion of many materials, including both metallic elements and certain alloys [4]. In addition, approximate values of the thermal expansion properties of some metallic elements can be obtained from theoretical considerations. For ex-

ample, using a monatomic model with central-force interactions between nearest neighbors, MacDonald and MacDonald [5] have calculated values of the linear thermal expansion at temperature T relative to that at reference temperature T_{ref}

$$\epsilon(T, T_{\text{ref}}) = [L(T) - L(T_{\text{ref}})] / [L(T_{\text{ref}})] \quad (1)$$

and of the coefficient of linear thermal expansion

$$\begin{aligned} \alpha(T, T_{\text{ref}}) &= d/dT \epsilon(T, T_{\text{ref}}) \\ &= [dL(T) / dT] / [L(T_{\text{ref}})] \end{aligned} \quad (2)$$

for several metallic elements occurring in the face-centered cubic structure.

Despite the availability of either calculated or nominal measured values for the thermal expansion of the types of materials used in constructing a high-temperature gas thermometer, it is prudent for those who are interested in realizing the Kelvin Thermodynamic Temperature Scale by high-temperature gas thermometry to measure the thermal

About the Authors: All are with the Center for Basic Standards in NBS' National Measurement Laboratory.

¹Figures in brackets indicate literature references.

expansion on samples of the actual materials from which the gas bulb and capillary are to be fabricated, especially if these materials are alloys. The reason for this admonition is the great sensitivity, mentioned above, of the thermodynamic temperature determination to the thermal expansion of the gas-containing components.

There are several methods in use for the measurement of linear thermal expansion, ranging in sensitivity $\delta L/L$ from 10^{-5} to 10^{-11} . Particular attention has been paid to the low-temperature region because of theoretical interest in deviations from the simple Grüneisen relation [6,7]. Existing methods include optical interferometry [8–10], x-rays [11], and the electrical measurement of capacitance of inductance [12,13].

This paper reviews the construction of a thermal expansion apparatus that permits measurement of length changes at the 1 ppm level of accuracy and determination of sample temperatures that are accurate within 0.01 °C. In addition, the results of thermal expansion measurements are reported for high-purity Pt and for two Pt-Rh alloys. The results of our measurements are analyzed in such a manner as to permit straightforward calculation of the quantities defined by eqs (1) and (2) and ready comparison with the results of other workers. The present experiments were performed in support of the National Bureau of Standards Gas Thermometry Program. Measurements were made over the range -27 °C to 570 °C. The method selected for the measurements was that of optical interferometry.

2. Experimental

2.1 Thermal Expansion Furnace

The thermal expansion furnace used in these experiments was designed in its original form by the late H. F. Stimson. Details of its present construction were provided by L. A. Guildner, former head of the NBS Gas Thermometry project, who also supervised its fabrication and the acquisition of the data discussed in this report. The thermal expansion apparatus was designed for use over the range -30 °C to $+700$ °C. Of paramount importance was the attainment of temperature homogeneity within 0.01 °C over the volume occupied by the sample. It was necessary, of course, to provide a light path for the interferometric measurements and to allow the accurate measurement of the sample temperature. Accomplishment of these objectives required the multi-chambered, sealed furnace that is shown in cross section in figure 1.

The use of several radiation shields and structural shells to improve temperature homogeneity within a cryostat or furnace is a well-established technique; in this case, shell I1 carries the main heater assembly, a group of five independent resistive units. Shells I2 and I3 also are equipped with heaters, as noted in the caption of figure 1.

Differential thermopiles allow direct comparison of the temperatures of the top plate of I1, the upper portion of its side wall, the middle portion of its side wall, and the lower portion of its side wall with that of its bottom plate. Similarly, the temperatures of the top plate and the side wall of I2 can be compared with that of its bottom plate. Finally, a thermopile also was installed on the surface of shell I3. Use of these thermopile circuits assists the operator in attempting to minimize internal temperature gradients.

Both the quartz window and the platinum resistance thermometer are sealed into the furnace by O-rings. As noted in figure 1, the furnace can be evacuated so that the operator can vary the pressure and type of gas in the furnace.

2.2 Interferometer

The linear thermal expansion of each sample was determined by the Fizeau interferometer method described by Candler [15] and Merritt [16] and refined by Saunders [17]. In fact, the optical instrument used in this work was one formerly used by Saunders, but modified by the substitution of a ^{198}Hg light source in place of the original helium lamp. A schematic drawing of the optical arrangement is given in figure 2.

The principle of the Merritt-Saunders thermal expansion determination is not complex, and it has the further advantage of usefully high precision. A lamp, in this case a low-pressure ^{198}Hg , electrodeless, water-cooled tube excited by microwave energy, provides light that is collimated by a lens L, then dispersed by a prism DP in order to restrict its wavelength range to that of the ^{198}Hg line at 546.2 nm. The light reflected by the two inner faces of the glass plates A and B forms an interference pattern when viewed through the eyepiece E or when imaged on the film F. The interference pattern follows the relation

$$N \lambda_0 = 2 n L \cos \Theta \quad (3)$$

where N is the number of fringes, λ_0 is the vacuum wavelength in μm of the incident light, n is the index of refraction of the medium between the plates, L is the separation of the plates in μm , and

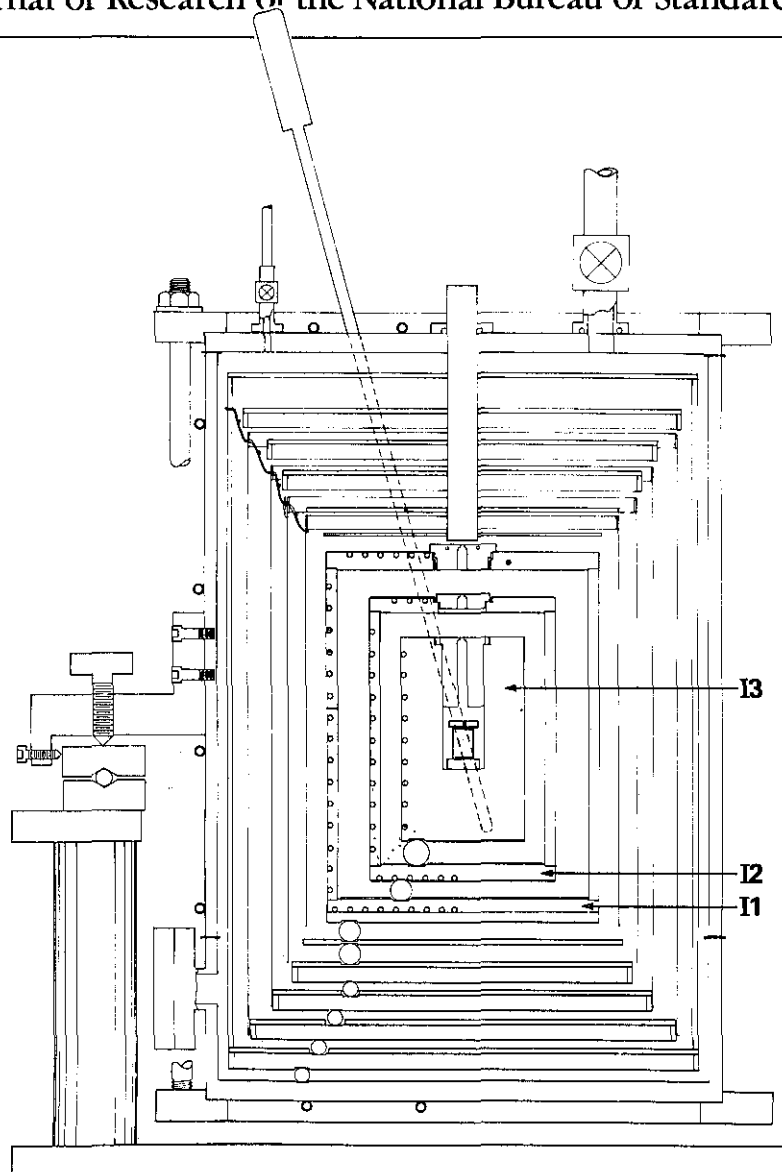


Figure 1—Schematic drawing of the thermal expansion furnace. The outermost shell, made of brass, is sufficiently strong so as to permit evacuation of the furnace. The brass shell also can be cooled to -30°C by virtue of cooling coils on its exterior surface. Inside the brass shell is a radiation shield made of copper. The three shields immediately within the copper one are made of silver in order to provide surfaces of high radiant reflectivity. A highly reflective gold foil shield, supported at the top and bottom by "Inconel 600"[14] plates, surrounds the largest of three Inconel shells. The silver and gold radiation shields are constructed with separate side walls which are suspended by hook-and-eye sets, beginning with hooks set into the copper shield, as shown in the figure. The Inconel shell, I1, is equipped with separate resistive heaters placed in grooves in its top, bottom, upper sidewall, mid-

dle sidewall, and lower sidewall. The middle Inconel shell, I2, was prepared with three heater circuits located on its top plate, its sidewall, and its bottom plate. The innermost shell, I3, has a single heater on its sidewall. I3 was prepared from a solid, 7.5 cm diam by 13 cm long block of Inconel; a central hole was bored in it for enclosure of the sample assembly, and a diagonal hole was bored in its body as a socket for a platinum resistance thermometer. In the text, shell I3 is also identified as the sample tempering block. The bottom plates of the shields and Inconel shells rest upon sets of three steel ball bearings that are located in slots in the next lower plate; this technique provides a low-thermal-conductivity, yet a strong and flexible support for the furnace. The brass outer shell was assembled in three sections—a top plate, a cylindrical side wall, and a bottom plate. Polytetrafluorethylene gaskets,

compressed by a set of screw clamps, provide the primary vacuum seal for the brass shell. The furnace is leveled and positioned by three sets of screws as shown. These screws make contact with a ball race that is rigidly fixed to the laboratory bench. Three-element "Platine"[14] thermopiles are arrayed on the I1, I2, and I3 surfaces. These thermopiles are connected in differential circuits for use in temperature control. A quartz window, 1.9 cm diam and 16 cm long, is sealed in place above the sample and the interferometer plates. Insertion of a sample into the furnace is accomplished by removal of the top plate of the brass shell. The top plates of the radiation shields are interconnected by "Inconel X"[14] wires, so that all of these top plates are removed as a unit. Removal of the plugs in the Inconel shells I1, I2, and I3 then permits removal and replacement of the sample assembly.

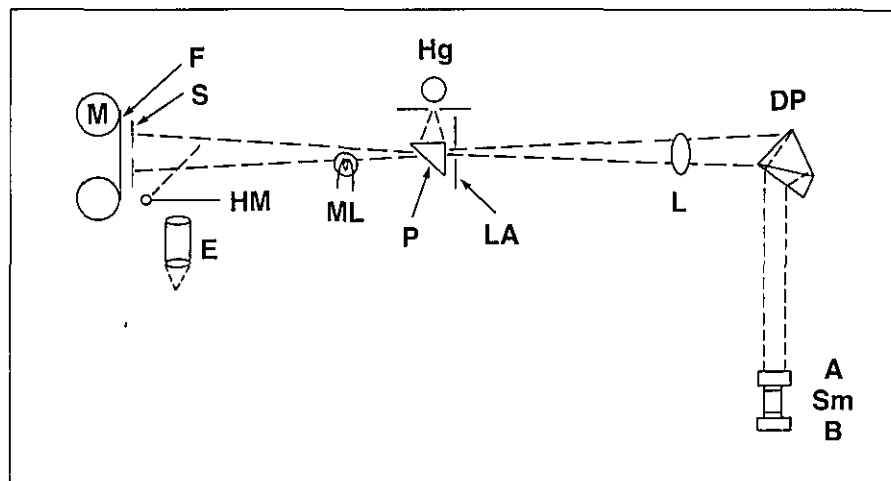


Figure 2—The recording interferometer schematically. M—Film drive motor. F—Film. S—Slit. HM—Hinged mirror. E—Eyepiece. ML—Marker lamp. Hg—¹⁹⁸Hg lamp. P—Simple prism. LA—Limiting aperture. L—Collimating lens. DP—Double dispersion prism. A,B—Interferometer plates. Sm—Sample.

Θ is the angle between the incident light rays and the normal to the lower reflecting surface atop the sample.

Furthermore, as the sample expands or contracts with changes in its temperature, the interference pattern undergoes a corresponding change because L changes. By imaging the interference pattern on the film, the operator can obtain a permanent record for later evaluation. The eyepiece can be used in conjunction with the hinged mirror HM to observe the proper alinement of the optical system. In order to avoid the presence of unwanted interference effects, it is necessary that the upper surface of the top interferometer plate A form an angle—in this case $20'$ —with respect to the interfering surfaces. Similarly, it is necessary to tilt slightly the lens and the dispersing prism so as to eliminate any interference effects from them.

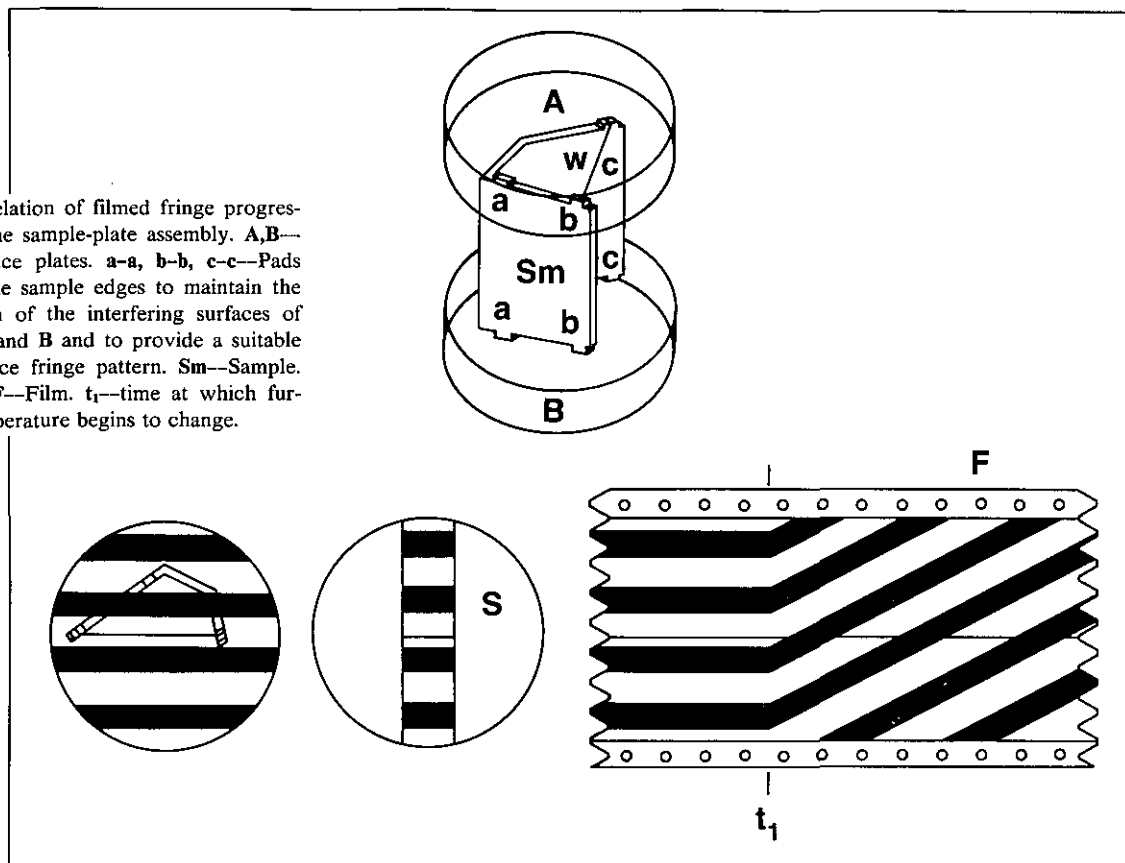
If the two interfering surfaces of the sample assembly plates A and B were to be made exactly parallel, then the interference pattern would consist of a single broad fringe. In that case, the viewer would see the entire assembly lighten and darken as the sample length expanded or contracted. In the Merritt-Saunders method, however, the upper interfering surface, shown in figure 3 as the underside of plate A, is caused to tilt slightly in order to provide several parallel interference fringes. This tilting is arranged by making the sample length at the location of the pads a-a either longer or shorter than it is at the location of the pads b-b and c-c. From eq (3), it can be deduced that the difference in the number of fringes at the two edges of the sample assembly, ΔN , depends upon the difference in separation of the two interfering surfaces at their edges, ΔL , according to the relation $\Delta N = 2n \Delta L \cos \Theta / \lambda_0$. In this manner, the changing position of the fringe pattern with respect to the fiducial mark

can be determined with a resolution that is substantially better than ± 1 fringe. The fiducial mark is provided by a fine Pt wire W that is fastened onto the sample between upper pads b and c.

The fringe pattern that is obtained from a properly alined optical system is shown in figure 3. The circular diagram on the lower left of figure 3 shows the pattern as seen by the operator while viewing through the eyepiece before assembly of the slotted plugs in I1, I2, and I3. We have found that the fringe pattern appears to change position slightly with respect to the fiducial mark as the optical aperture is decreased to sharpen the fringe image. It is necessary during this process also to adjust the position of the furnace so that the fringe image does not disappear entirely.

The lower middle diagram shows the fringe pattern as it appears at the film plane after partial masking by the slits in the plugs of shells I1-I3 and the slit S. Note that the position of the fringe pattern can readily be measured with respect to the fiducial mark provided by the wire W. During measurements the operator correlates the position of the film with the measured furnace temperature, making use of the known rate of film advance and tagging the film record at known times by use of the marker lamp ML. The film drive motor M is activated during any change in furnace temperature and for some time while a new temperature is being measured. The lower right diagram shows a typical filmed record of the fringe pattern. At the time t_1 , a change in the furnace temperature is signaled by deviation of the fringe pattern from the direction parallel to the fiducial mark. By counting the fringes as they pass the fiducial mark, the operator can follow the progress of the sample thermal expansion.

Figure 3—Relation of filmed fringe progression to the sample-plate assembly. A,B—Interference plates. a-a, b-b, c-c—Pads left on the sample edges to maintain the separation of the interfering surfaces of plates A and B and to provide a suitable interference fringe pattern. Sm—Sample. S—Slit. F—Film. t_1 —time at which furnace temperature begins to change.



2.3 Sample Assembly

The thermal expansion measurements were performed on samples made either from surplus materials used in constructing gas bulbs for the NBS Gas Thermometer or from pieces cut from used gas bulbs. Most material was about 1 mm thick.

The general shape of the samples is shown in figure 3. After cutting the material into a strip 22–25 mm by ~50 mm, re-cutting it so as to produce three sets of pads as shown in the figure, and bending it into the desired shape, a 0.08 mm platinum wire was wedged tightly in place into thin grooves in the sample pads b and c as a fiducial marker. The sample was annealed in He gas at 1100 °C for 1 h.

Circular optical flats of fused silica were used to generate the interference fringe pattern. The upper plate (A, figs. 2 and 3), was 2.2 cm in diam and 0.4 cm thick. As mentioned above, it was cut with an angle of approximately 20' between its upper and lower surfaces so that no visible interference pattern would occur as a result of reflections from its upper surface. The lower plate (B, figs. 2 and 3), was 2.4 cm in diam and 0.7 cm thick. The lower surface of plate A and the upper surface of B were

coated with TiO_2 so as to optimize the performance of the optical system (i.e., total reflection by the upper surface of B, ~30% reflectivity by the lower surface of A). The bottom surface of plate B was frosted so as to eliminate any interference therefrom.

The lengths between pairs of sample pads were measured using gage blocks and a precision micrometer of 2.6 cm capacity. By wringing together a suitable set of gage blocks, the operator could closely approximate the distance separating the surfaces of paired sample pads. Careful trimming and polishing of the pads, combined with micrometer measurement in a controlled temperature environment allowed the operator to measure and match the two sets of pads b-b and c-c within 0.25 μm . The separation between pads a-a was purposely made about 1 μm longer than for the other two sets in order to provide the necessary angle between the reflecting surfaces of plates A and B to generate three or four fringes, as noted above.

2.4 Thermometry

The temperature of the sample chamber is determined through the use of a specially-made plat-

inum resistance thermometer (PRT) of $R(0\text{ }^{\circ}\text{C})$ about $2.5\ \Omega$. The four-lead resistor element is made of high-purity platinum wire of 0.13 mm diam wound in the form of a bifilar, simple helix. The protective sheath is made of synthetic vitreous silica; it is 40 cm long, 7 mm diam. The thermometer is filled with a mixture of gases; 90% Ar, 10% O_2 . Thermometers made in this manner can be calibrated according to the procedures recommended in the text of the 1968 International Practical Temperature Scale [18] so as to provide IPTS-68 temperatures that are accurate within $\pm 0.002\text{ }^{\circ}\text{C}$ from $0\text{ }^{\circ}\text{C}$ to $630\text{ }^{\circ}\text{C}$. Moreover, they can be used at temperatures as high as $1100\text{ }^{\circ}\text{C}$ with levels of imprecision as low as $\pm 0.02\text{ }^{\circ}\text{C}$. The resistance values of the thermometer used in the thermal expansion apparatus were obtained by means of an ac resistance bridge designed by Cutkosky of the NBS [19].

In practice, the thermometer was calibrated in the NBS Platinum Resistance Thermometry Calibration Laboratory at the triple point of water, at the tin freezing point and at the zinc freezing point. The usual relations were then employed to obtain values of temperature on the IPTS-68 in the range $-27\text{ }^{\circ}\text{C}$ to $630\text{ }^{\circ}\text{C}$. This range was sufficient to satisfy the needs of this experiment. Possible drift in the thermometer calibration was monitored by periodic re-calibration at the water triple point in the Gas Thermometry Laboratory. We estimate the uncertainty in the thermometer calibration as no larger than $\pm 0.001\text{ }^{\circ}\text{C}$.

Uncertainty in the measured sample temperature also can arise from consideration of possible temperature gradients between the sample and its tempering block and between the block and the thermometer itself. We discuss these problems in some detail in section 4.

2.5 Temperature Control

Control of the furnace temperature is achieved by use of differential thermocouples that are mentioned above, together with the platinum resistance thermometer. There are five independent heaters located on shell I1, three on shell I2, and one on shell I3 (this shell also is referred to as the sample tempering block); at any particular sample temperature, apportioning the required heat among these nine heaters is a complicated problem. Preparatory to making measurements at a particular temperature, the operator can adjust power to the heaters so as to minimize gradients within the shells I1 and I2. The temperatures of I1, I2, and I3 also can be adjusted to approximate equality. Finally, the operator can attempt to demonstrate temperature ho-

mogeneity within the tempering block by changing the position of the platinum resistance thermometer. Any variation in its reading can arise from inadequate heater adjustment or from a more pernicious cause, inadequate thermal isolation from the room environment. Use of a special heater, not shown in figure 1 but located along the thermometer guide tube, allows the operator to evaluate the quality of the thermometer tempering.

In practice, the block I3 was supplied with a small extra amount of heat from its heater in order to maintain its temperature slightly above that of shell I2. In turn, shell I2 was maintained at a temperature slightly above that of shell I1. The overall objective was to apportion the power to the nine heaters so as to minimize the apparent gradient along block I3.

All thermopile *emf* values were measured with a calibrated strip-chart recorder.

2.6 Measurement Procedures

In performing a determination of the thermal expansion of a particular sample, the first step consisted of preparing a sample assembly capable of providing reasonably straight interference fringes arrayed perpendicular to the slit in front of the camera, as noted above. The sample lengths at pads a-a, b-b, and c-c were recorded, as was the temperature at which the measurement was performed.

Once the sample assembly was installed in the apparatus, the slotted plugs in shells I3, I2, and I1 and the shield covers were replaced and the furnace was evacuated prior to refilling with ^4He gas at a suitable pressure.

Sample temperatures were chosen with regard to the expected complexity of the curve of the thermal expansion coefficient vs temperature. Cooling below $0\text{ }^{\circ}\text{C}$ was accomplished by Freon refrigerant flowing through the coils surrounding the outer brass shield. For temperatures above $0\text{ }^{\circ}\text{C}$, the voltages applied to the Inconel shell heaters were varied until the platinum resistance thermometer showed a resistance corresponding to the chosen temperature and until the temperature gradient within block I3 was minimized. Because of the long thermal response time of the apparatus, the time required to pass from one temperature to another one sometimes reached 24 hours.

The filmed fringe pattern that was obtained at each stable temperature was examined using a microdensitometer in order to determine the fractional fringe count at the fiducial mark to the nearest 0.001 fringe. Other experimental data recorded while the temperature was stable in-

cluded the resistance of the sample PRT; the resistance of a temperature-controlled standard resistor (used in monitoring the stability of the resistance bridge); and the pressure of the ^4He gas in the apparatus.

During the time that the apparatus temperature was changing, the interferometer film system recorded the changing fringe pattern that resulted from the changing length of the sample. Evaluation of this film generally allowed a determination to be made of the whole number of fringes that passed the image of the fiducial mark during the corresponding temperature change. In certain cases, the recording system failed to operate; then the integral number of fringes involved in the measurement was estimated by means to be discussed in the next section.

2.7 Analysis of Data

In order to analyze our experimental data, we prepared tables that are keyed to the stable temperature values in chronological order. For each temperature, we listed the measured fractional fringe value associated with the position of the fiducial mark as well as the pressure of ^4He gas in the apparatus. We also listed the observed overall change in fringes, ΔN_i , that accompanied each temperature change, Δt_i . These entries constitute the experimental data set for each sample.

In the relatively few cases in which the fringe-recording system failed to operate during a change to a new temperature setting, we obtained an approximate value of the fringe change from a plot of $\Delta N_i/\Delta t_i$ vs the mean temperature of the interval. Such a plot was found to yield unambiguously the integral value of fringes passing the fiducial mark during a temperature change.

It is necessary to correct our fringe measurements for the effect of the index of refraction of the ^4He gas. This can be accomplished according to the relation

$$\delta N(t_i)_{\text{vac-meas}} = 2 L_i \cos \Theta (1 - n_i) / \lambda_0 \quad (5)$$

where $\delta N(t_i)_{\text{vac-meas}}$ are the changes in the measured fringe counts at t_i when corrected to vacuum conditions; the L_i are the sample lengths at t_i expressed in meters; $\cos \Theta$ is essentially unity; λ_0 , the vacuum wavelength of the ^{198}Hg line used in the experiment, is 546.2271×10^{-9} m [20]; and the n_i are the indices of refraction of the ^4He gas contained in the apparatus at t_i . The n_i can be calculated for each experimental temperature and pressure from the relation [21]

$$n_i = 1 + (3.5 \pm 0.1) \times 10^{-5} \left[\frac{p_i}{101} \right] \left[\frac{293}{t_i + 273} \right] \quad (6)$$

where p_i is expressed in kPa and t_i in degrees Celsius. It was sufficient to use L_{meas} in place of L_i since in no case was $\delta N(t_i)_{\text{vac-meas}}$ larger than 0.05 fringe.

Once we had corrected the observed fringe measurements for the presence of the ^4He gas, we could prepare a set of corrected values of $\Delta N(t_i, t_{i+1})$ suitable for fitting.

We assumed that the linear thermal expansion of a particular sample, relative to 0°C and expressed in experimental fringe units, could best be represented by a polynomial of the form

$$N(t) = N(0^\circ\text{C}) + \sum_{n=1}^m A_n t^n \quad (7)$$

where t is temperature in degrees Celsius.

The coefficients A_n of eq (7) can be evaluated by fitting the function

$$\Delta N(t_i, t_{i+1}) = \sum_{n=1}^m A_n (t_i^n - t_{i+1}^n) \quad (8)$$

to the experimental data. The coefficient $N(0^\circ\text{C})$ is subsequently obtained as

$$N(0^\circ\text{C}) = N(t_{\text{meas}}) - \sum_{n=1}^m A_n t_{\text{meas}}^n \quad (9)$$

where $N(t_{\text{meas}})$ is the length of the sample as measured at the known temperature t_{meas} and expressed in experimental fringe units.

We fitted the corrected data for each sample, using eq (8) in a least-squares computational program with up to six coefficients. For each successive polynomial ($m=2, 3, \dots, 6$) the program provided an estimated standard deviation of the fit and an analysis-of-variance test of the significance of the m th coefficient [22]. This test provided us a useful criterion for selecting the degree of the polynomial that best fitted the data.

In fitting the data we gave zero weight to all points involving temperature changes less than 2°C . In every such case, however, these data points are included in the tables and plotted in the figures.

We arranged eq (7) to obtain the equation for the linear thermal expansion relative to 0°C expressed in the form of eq (1).

$$\epsilon(t, 0^\circ\text{C}) = [L(t) - L(0^\circ\text{C})] / L(0^\circ\text{C})$$

$$\begin{aligned}
 &= [N(t) - N(0^\circ\text{C})] / N(0^\circ\text{C}) \\
 &= \sum_{n=1}^m [A_n / N(0^\circ\text{C})] t^n \quad (10)
 \end{aligned}$$

For any other reference temperature, $\epsilon(t, t_{\text{ref}})$ can be obtained as

$$\epsilon(t, t_{\text{ref}}) = \frac{\epsilon(t, 0^\circ\text{C}) - \epsilon(t_{\text{ref}}, 0^\circ\text{C})}{1 + \epsilon(t_{\text{ref}}, 0^\circ\text{C})}. \quad (11)$$

Frequently, the experimental results are presented in the literature using a reference temperature of 293 K (i.e., 19.85 °C) and using temperatures expressed in kelvins [4]. For each sample, we present equations in this format using eq (11) to derive the appropriate coefficients.

3. Results

Thermal expansion data have been determined for three samples of 1 mm thickness; platinum sheet (Englehard Industries 99.95%) [14], an alloy of nominal composition (88 wt% Pt+12 wt% Rh), and an alloy of nominal composition (80 wt% Pt+20 wt% Rh).

3.1 100% Pt Sample

As described above, the sample length at each set of pads (a-a, b-b, and c-c, fig. 3) was determined by the use of a calibrated gage block and a precision dial micrometer. The sample lengths were measured relative to the gage block at 22 °C. Since the gage block had been calibrated at 20 °C, to obtain the true lengths of the sample at 22 °C, it was necessary to adjust the gage block length for the actual temperature difference. The sample lengths at pads b-b and c-c agreed within 130 nm. At pads a-a, the sample length was some 826 nm longer than the average length at the fiducial mark. The 22 °C average length at the fiducial mark as 25.277 090 mm \pm 130 nm. This corresponds to 92, 551.58 \pm 0.5 fringes in vacuum.

Data at 26 stable temperatures were recorded on the above sample using the Merritt-Saunders interferograph over the range -27.6°C to 567.7°C . The data were recorded as two runs (Nos. 205 and 206) because a lapse of nearly one month separated observations No. 17 and No. 18. However, the apparatus was not disturbed during that time and, herein, we treat the data as one set. Column 2 of table 1 lists the stabilized temperature points in chronological order. Note that the data were not obtained in a single sweep through the temperature range of interest.

As noted earlier, the filmed fringe pattern that was obtained at each stable temperature was examined using a microdensitometer in order to determine the fractional fringe count at the fiducial mark to the nearest 0.001 fringe. This fractional fringe count is noted in column 3 of the table for each point.

In column 4 of table 1, we have reported the pressure in kPa of the ^4He gas that filled the thermal expansion apparatus during each stable temperature measurement. Using the refractive index for ^4He , adjusted for the actual furnace temperature and pressure by means of eq (6), we corrected the fractional fringe count in column 3 of table 1 to vacuum conditions by use of eq (5). These corrected values are given in column 5.

The corrected differences in total fringe count between successive stabilized temperatures, are given in column 6 of table 1. Note that each entry in column 6 is placed between the two relevant entries for the stable-temperature points in columns 1-5.

As noted in section 2.7, we used a polynomial of the form of eq (8) to fit the values of $\Delta N(t_i, t_{i+1})$ by the method of least squares. A summary of the fitting parameters is given in table 2. As indicated in table 2, the analysis-of-variance test for significance of the last coefficient showed the coefficient of the 4th degree term of the polynomial to be significant at the 95% level of confidence.

Using the 4th-degree coefficients given in table 2, we calculated values of ΔN for successive experimental end-point temperatures; these are given in column 7 of table 1.

In column 8 of table 1 are listed the differences ($\Delta N_{\text{expt}} - \Delta N_{\text{calc}}$). These differences are plotted against the average sample temperature $(t_i + t_{i+1})/2$ in figure 4.

Using the relationship expressed by eq (10), the percent linear thermal expansion for 100% Pt with 0 °C as the reference temperature is given by eq (12) where $N(0^\circ\text{C}) = 92,533.46$ fringes.

$$\begin{aligned}
 100 \epsilon(t, 0^\circ\text{C}) &= 100 \sum_{n=1}^4 [A_n / N(0^\circ\text{C})] t^n \\
 &= 8.862 \times 10^{-4} t + 1.760 \times 10^{-7} t^2 \\
 &\quad - 1.144 \times 10^{-10} t^3 \\
 &\quad + 8.93 \times 10^{-14} t^4. \quad (12)
 \end{aligned}$$

Table 1. Experimental Data for 100 Wt% Pt.

$N(22\text{ }^\circ\text{C})=92,551.58\pm 0.5$ fringes

1	2	3	4	5	6	7	8
Point No.	$t(68),\text{ }^\circ\text{C}$	F.F. ^a	Gas Pressure kPa	F.F. corr.	ΔN_{expt}^b	ΔN_{calc}^c	Dev,fr ^f
Run 205							
1	567.685	.930	0.73	.922			
1a					-32.267	-32.330	.063
2	533.950	.664	0.73	.655			
2a					-76.384	-76.277	-.107
3	453.083	.281	0.73	.271			
3a					(-14.064) ^c	-14.332	.268
4	437.694	.216	0.67	.207			
4a					-94.490	-94.592	.102
5	334.599	.727	0.67	.717			
5a					-.127 ^d	-.006	-.121
6	334.592	.600	0.67	.590			
6a					-63.933	-63.786	-.147
7	263.548	.669	0.67	.657			
7a					-84.052	-84.038	-.014
8	167.911	.619	0.67	.605			
8a					-48.195	-48.264	.069
9	111.803	.426	0.67	.410			
9a					-30.260	-30.216	-.044
10	76.173	.168	0.67	.150			
10a					-16.703	-16.833	.130
11	56.139	.466	0.67	.447			
11a					-24.172	-24.267	.095
12	27.006	.292	0.53	.275			
12a					(-12.018)	-11.893	-.125
13	12.613	.277	0.60	.257			
13a					(6.239)	6.228	.011
14	20.160	.515	0.60	.496			
14a					(-7.141)	-7.112	-.029
15	11.540	.375	0.60	.355			
15a					7.124	7.129	-.005
16	20.180	.498	0.60	.479			
16a					(7.990)	7.960	.030
Run 206							
17	29.794	.488	0.60	.469			
17a					(-47.120)	-47.077	-.043
18	-27.599	.372	0.60	.349			
18a					8.225	8.269	-.044
19	-17.422	.596	0.60	.574			
19a					6.784	6.819	-.035
20	-9.061	.382	0.67	.358			
20a					(-.019) ^d	-.017	-.002
21	-9.082	.363	0.67	.339			
21a					7.101	7.096	.005
22	-.412	.463	0.67	.440			
22a					7.042	7.052	-.010
23	8.175	.504	0.67	.482			
23a					(.989) ^d	1.071	-.082
24	9.477	.493	0.67	.471			
24a					7.221	7.212	.009
25	18.225	.714	0.67	.692			
25a					8.585	8.596	-.011
26	28.614	.298	0.67	.277			

^a F.F.; fractional fringe count at the fiducial mark.

^b ΔN_{expt} ; corrected differences in sample length, expressed in fringes.

^c Use of parentheses indicates that the integral number of fringes passing the fiducial mark during a particular temperature change was obtained from a trial plot of $\Delta N/\Delta t$ vs the mean temperature of the interval (see section 2.7).

^d Data points 5a, 20a, and 23a were given zero weight in the fitting procedure.

^e ΔN_{calc} ; fringe differences calculated for the end-point temperatures given in column 2, using eq (8) with the coefficients given in table 2.

^f Dev; $\Delta N_{\text{expt}} - \Delta N_{\text{calc}}$. These differences are plotted against the average experimental end point temperatures in figure 4.

Table 2. Fitting parameters for the thermal expansion of 100% Pt.

Equation used in least-squares fitting procedure:

$$\Delta N(t_i, t_{i+1}) = \sum_{n=1}^m A_n (t_i^n - t_{i+1}^n) \quad (8)$$

 Determination of number of polynomial terms m for "best fit":

 $p=22$ data points

m	σ^a	F_m^b	$F_{0.95}(1, p-m)$
1	1.729 0	—	—
2	0.125 4	4537.7	4.35
3	0.110 1	7.7	4.38
4	0.098 5	6.5	4.41
5	0.098 7	0.9	4.45
6	0.099 0	0.9	4.49

Coefficients of 4th degree polynomial:

n	A_n	σ of A_n
1	0.819 987 6	0.001 441 2
2	0.000 162 877	0.000 012 011
3	-0.000 000 105 857	0.000 000 036 848
4	0.000 000 000 082 658	0.000 000 000 034 522

 $N(0^\circ\text{C})=92,533.46$ fringes [from eq (9)]

^a σ ; the estimated standard deviation of the fit.

^b F_m ; an index used to estimate the level of significance of the m th coefficient in the equation fitted to the data.

$$F_m = 1 + (p - m + 1) \left[\left(\frac{\sigma_{m-1}}{\sigma_m} \right)^2 - 1 \right]$$

where p is the number of data points and m is the number of coefficients in the polynomial. The coefficient A_m is considered significant at the desired level of confidence if F_m is greater than the corresponding value given in the fourth column. (Entries in column 4 were taken from a standard table for the F -distribution, e.g., table III of [22].)

For a reference temperature of 293 K the corresponding equation is

$$\begin{aligned} 100 \epsilon(T, 293 \text{ K}) = & -1.766 \times 10^{-2} \\ & + 8.860 \times 10^{-4} (T - 273.15) \\ & + 1.760 \times 10^{-7} (T - 273.15)^2 \\ & - 1.144 \times 10^{-10} (T - 273.15)^3 \\ & + 8.93 \times 10^{-14} (T - 273.15)^4. \end{aligned} \quad (13)$$

3.2 (88 wt% Pt + 12 wt% Rh) Sample

The (88 wt% Pt + 12 wt% Rh) sample was made with a geometric shape similar to that of the 100%

Pt sample. The sample length at the position of the fiducial wire was measured against a gage block, again using a precision dial micrometer; the sample length was determined to be $21.039\,689 \text{ mm} \pm 105 \text{ nm}$ at 26.7°C , which corresponds to $77,036.42 \pm 0.4$ fringes in vacuum.

Thirty-seven stable temperature points were obtained on the (Pt + 12% Rh) sample in two sets of measurements that were separated in time by four months. Table 3 shows the data in the same format as that presented in table 1 for 100% Pt, with the two sets of measurements separated for analytical purposes. Again it was necessary to deduce the integral number of fringes that crossed the fiducial mark in a few cases; these estimated values are enclosed in parentheses in column 6.

We note that the analysis of two independent sets of thermal expansion data can help considerably to illuminate the overall level of reproducibility of our measurements. In principle, the thermal expansion data in the second set of measurements should duplicate the data in the first set; the sample, though removed from the apparatus, was not modified between measurements. Only an accidental sample length change owing to rough handling, a modification of the sample properties owing to the heating that occurred during the first measurement, or a mis-alignment of the optical system during re-assembly of the apparatus should cause any discrepancy between the two sets of data. Realizing these possibilities, we fitted the thermal expansion data for each data set separately as well as grouped into one large data set.

The values ΔN_{calc} listed in column 7 of table 3 were obtained by the use of the fitting coefficients given in table 4, along with the experimental end-point temperatures. The differences ($\Delta N_{\text{expt}} - \Delta N_{\text{calc}}$) are listed in column 8 of table 3 and they are plotted in figure 5.

Although the analysis-of-variance test indicates that a fifth term is statistically significant even at the 99% confidence level, we choose to represent our data with a four-term equation. There are two reasons for making this choice. The first is that the observed data of Run 204 (15 of the 34 points which cover over 90% of the temperature range) can be unambiguously "best fitted" by a four-term equation from which the estimated standard deviation of the data is 0.018 fringe. The two data points from Run 207 which overlap the temperature range of Run 204 deviate by less than 0.005 fringe from the four-term equation fitted to Run 204. The 19 data points of Run 207 can be "best fitted" by a three-term equation from which the estimated standard deviation of the data is 0.020 fringe, a value

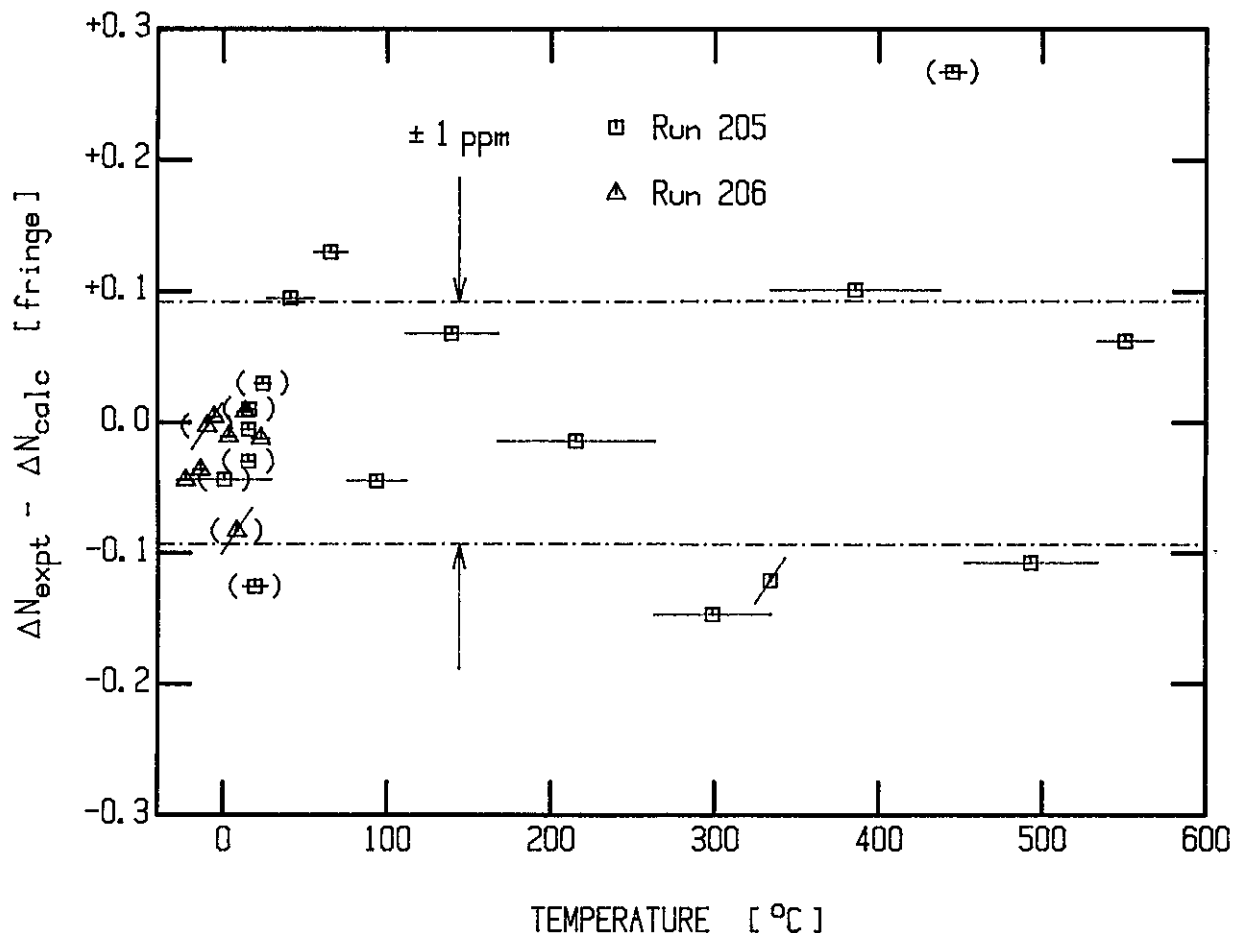


Figure 4—Differences in fringes of light at 546 nm between the length changes that were observed experimentally for 100% Pt and those that were calculated from the 4th degree fitting equation (see table 2). The squares indicate data of Run No. 205; the triangles, Run No. 206. The horizontal bar centered on each point denotes the temperature interval over which the length change was measured. () encloses a data point for which the whole number of fringes was estimated. / marks a data point that was given zero weight in the fitting process. — · — · — indicates the bounds of one part per million in sample length.

comparable to that obtained when a five-term equation is fitted to all of the data. It appears that the imprecision of the data below 25 °C allows an additional flexibility in the fitting process. This additional flexibility was also observed when the data for each of the three samples were fitted by two other model equations, indicating that there may be an unusual distribution of these data—though at a low level of imprecision.

The second reason for our choice of the four-term equation is to maintain a consistent treatment of the data for each of the three samples. By so doing, we believe that the comparison of the differences between the calculated values for the thermal expansion of pure platinum and the two rhodium-platinum alloys will be least influenced by the analytical treatment of the experimental data. The consequences of choosing the four- rather than the five-term equation are very slight. In the range -20 to 550 °C, no value of linear expansion relative

to 0 °C calculated with the four-term equation differs by as much as 1 ppm from that calculated with the five-term equation. This difference is less than the estimated uncertainty in the calculated value. The difference between the five- and four-term equation is indicated by the dotted line in figure 5.

We suggest that the percent linear thermal expansion relative to 0 °C, for (88 wt% Pt+12 wt% Rh) be calculated using the relation

$$\begin{aligned}
 100 \epsilon(t, 0^\circ\text{C}) &= 100 \sum_{n=1}^4 [A_n / N(0^\circ\text{C})] t^n \\
 &= 8.763 \times 10^{-4} t + 2.116 \times 10^{-7} t^2 \\
 &\quad - 1.455 \times 10^{-10} t^3 \\
 &\quad + 1.036 \times 10^{-13} t^4 \quad (14)
 \end{aligned}$$

where $N(0^\circ\text{C}) = 77,018.29$ fringes.

Journal of Research of the National Bureau of Standards

Table 3. Experimental data for (88 wt% Pt+12 wt% Rh).

$N(26.7\text{ }^\circ\text{C})=77,036.42\pm 0.4$ fringes

1	2	3	4	5	6	7	8
Point No.	$t(68)$, $^\circ\text{C}$	F.F. ^a	Gas Pressure kPa	F.F. corr	ΔN_{expt} ^b	ΔN_{calc} ^c	Dev, fr ^f
Run 204							
1	25.067	.288	0.93	.265			
1a					6.365	6.335	.030
2	34.325	.653	0.93	.630			
2a					6.953	6.936	.017
3	44.418	.605	0.93	.583			
3a					6.763	6.753	.010
4	54.202	.367	0.93	.346			
4a					7.216	7.224	-.008
5	64.624	.583	0.93	.562			
5a					6.892	6.890	.002
6	74.522	.474	0.93	.454			
6a					8.132	8.105	.027
7	86.115	.605	0.93	.586			
7a					13.740	13.753	-.013
8	105.668	.350	1.20	.326			
8a					20.269	20.254	.015
9	134.207	.611	0.86	.595			
9a					48.855	48.896	-.041
10	201.962	.467	1.07	.450			
10a					37.785	37.805	-.020
11	253.366	.250	1.07	.235			
11a					38.123	38.115	.008
12	304.418	.374	1.20	.358			
12a					73.945	73.933	.012
13	401.427	.316	1.20	.303			
13a					44.341	44.329	.012
14	458.382	.658	1.40	.644			
14a					35.900	35.861	.039
15	503.804	.558	1.47	.544			
15a					38.693	38.728	-.035
16	552.193	.250	1.47	.237			
Run 207							
17	272.145	.374	0.53	.367			
17a					-70.819	-70.859	.040
18	175.678	.557	0.53	.548			
18a					(-103.421) ^e	103.372	-.049
19	28.981	.140	0.53	.127			
19a					(-31.551)	-31.588	.037
20	-17.700	.588	0.40	.576			
20a					3.545	3.577	-.032
21	-12.361	.132	0.40	.121			
21a					2.941	2.946	-.005
22	-7.974	.073	0.40	.062			
22a					3.368	3.347	.021
23	-3.001	.441	0.40	.430			
23a					3.889	3.920	-.031
24	2.807	.337	0.67	.319			
24a					6.926	6.912	.014
25	13.010	.262	0.67	.245			
25a					(7.076)	7.102	-.026
26	23.443	.334	0.53	.321			
26a					(1.085) ^d	1.051	.034
27	24.983	.419	0.53	.406			
27a					(-25.781)	-25.788	.007
28	-13.120	.635	0.33	.625			
28a					-6.437	-6.447	.010
29	-22.757	.192	0.13	.188			
29a					3.054	3.080	-.026
30	-18.147	.255	0.40	.242			
30a					3.262	3.251	.011
31	-13.292	.512	0.27	.504			
31a					2.806	2.845	-.039

(Continued)

Table 3 Continued. Experimental data for (88 wt% Pt+12 wt% Rh).

$N(26.7\text{ }^\circ\text{C})=77,036.42\pm 0.4$ fringes

1	2	3	4	5	6	7	8
Point No.	$t(68),\text{ }^\circ\text{C}$	F.F. ^a	Gas Pressure kPa	F.F. corr	ΔN_{expt}^b	ΔN_{calc}^c	Dev,fr ^f
32	-9.053	.318	0.27	.310			
32a					3.152	3.125	.027
33	-4.408	.469	0.27	.462			
33a					3.844	3.848	-.004
34	1.298	.313	0.27	.306			
34a					4.080	4.069	.011
35	7.315	.393	0.27	.386			
35a					6.735	6.743	-.008
36	17.248	.126	0.27	.121			
36a					8.295	8.316	-.021
37	29.436	.425	0.27	.416			

^a F.F.; fractional fringe count at the fiducial mark.

^b ΔN_{expt} ; corrected differences in sample length, expressed in fringes.

^c Use of parentheses indicates that the integral number of fringes passing the fiducial mark during a particular temperature change was obtained from a trial plot of $\Delta N/\Delta t$ vs the mean temperature of the interval (see section 2.7).

^d Data point 26a was given zero weight in the fitting procedure.

^e ΔN_{calc} ; fringe differences calculated for the end-point temperatures given in column 2, using eq (8) with the coefficients given in table 4.

^f Dev; $\Delta N_{\text{expt}} - \Delta N_{\text{calc}}$. These differences are plotted against the average experimental end-point temperatures in figure 5.

Table 4. Fitting parameters for the thermal expansion of (88 wt% Pt+12 Rh).

Equation used in least-squares fitting procedure:

$$\Delta N(t_i, t_{i+1}) = \sum_{n=1}^m A_n (t_i^n - t_{i+1}^n) \quad (8)$$

Determination of number of polynomial terms m for "best fit":

$p=34$ data points

m	σ^a	F_m^b	$F_{0.95}(1, p-m)$
1	1.408 7	—	—
2	0.091 2	8086.2	4.15
3	0.049 3	80.8	4.16
4	0.025 9	85.1	4.17
5	0.020 5	19.4	4.18
6	0.020 4	1.2	4.20

Coefficients of 4th degree polynomial:

n	A_n	σ of A_n
1	0.674 912 2	0.000 374 0
2	0.000 162 975	0.000 003 093
3	-0.000 000 112 026	0.000 000 009 268
4	0.000 000 000 079 830	0.000 000 000 008 789

$N(0\text{ }^\circ\text{C})=77,018.29$ fringes [from eq (9)]

^a σ ; the estimated standard deviation of the fit.

^b F_m ; an index used to estimate the level of significance of the m th coefficient in the equation fitted to the data.

$$F_m = 1 + (p - m + 1) \left[\left(\frac{\sigma_{m-1}}{\sigma_m} \right)^2 - 1 \right]$$

where p is the number of data points and m is the number of coefficients in the polynomial. The coefficient A_m is considered significant at the desired level of confidence if F_m is greater than the corresponding value given in the fourth column. (Entries in column 4 were taken from a standard table for the F -distribution, e.g., table III of [22].)

For a reference temperature of 293 K the corresponding equation is

$$\begin{aligned} 100 \epsilon(T, 293\text{ K}) = & -1.747 \times 10^{-2} \\ & + 8.761 \times 10^{-4} (T - 273.15) \\ & + 2.116 \times 10^{-7} (T - 273.15)^2 \\ & - 1.454 \times 10^{-10} (T - 273.15)^3 \\ & + 1.036 \times 10^{-13} (T - 273.15)^4. \end{aligned} \quad (15)$$

3.3 (80 wt% Pt+20 wt% Rh) Sample

The (80 wt% Pt+20 wt% Rh) sample was prepared in a manner similar to those used with the other two samples. Its length at 21 °C was determined as 21.380 463 mm \pm 107 nm, corresponding to 78,284.15 \pm 0.4 fringes in vacuum.

The 25 $\Delta N(t_i, t_{i+1})$ data points measured with this sample are displayed in table 5, using the same format that was employed for tables 1 and 3.

Again we used the method of least squares with a polynomial in t to fit the data in the form $\Delta N(t_i, t_{i+1})$. A summary of the fitting parameters is given in table 6. Note that the F test indicates significance of the t^4 term at the 95% level of confidence.

Using the fourth-degree coefficients given in table 6, we calculated values of ΔN for the experimental end-point temperatures, as we did with the other two samples, as well as the differences ($\Delta N_{\text{expt}} - \Delta N_{\text{calc}}$). These sets of values are given in

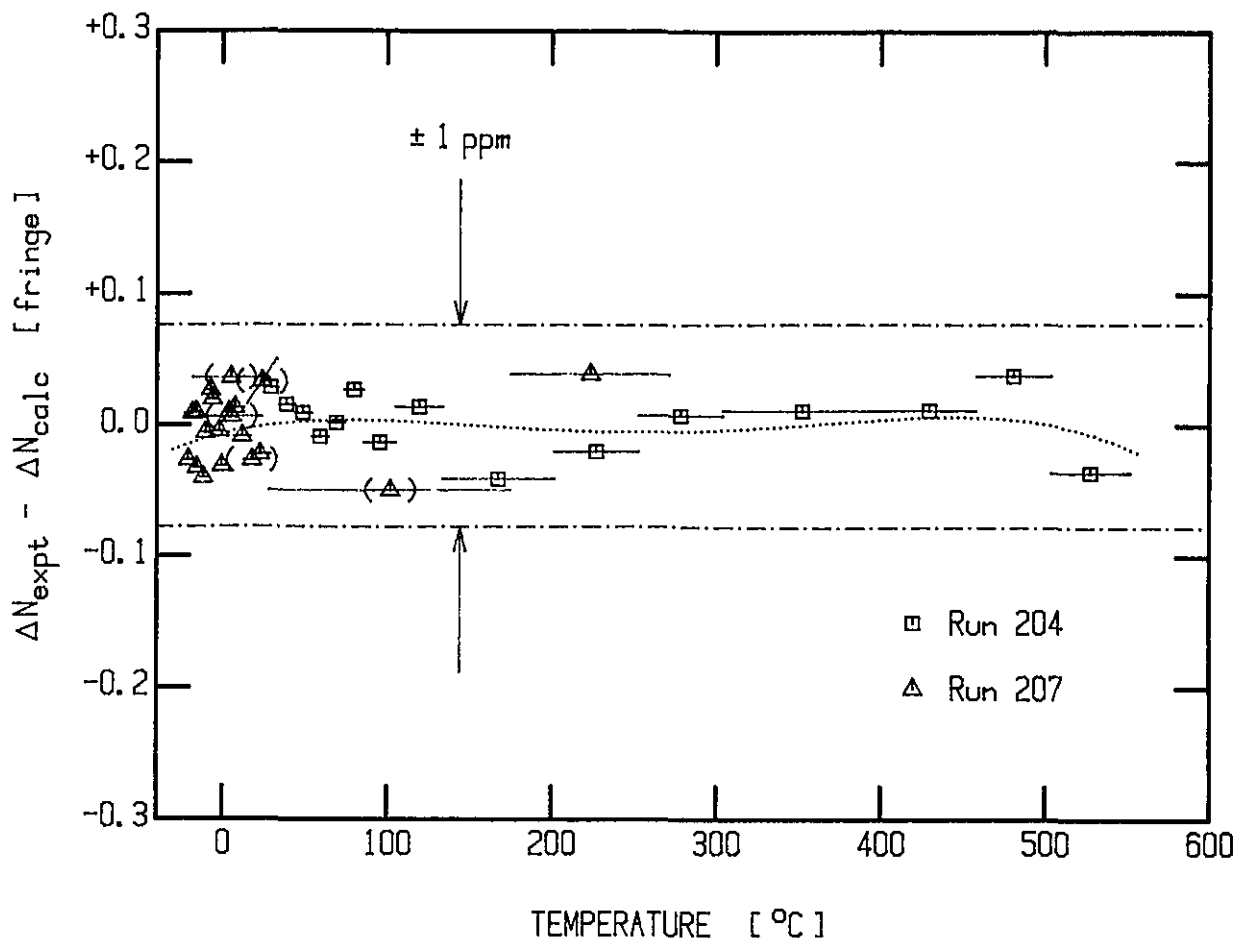


Figure 5—Differences in fringes of light at 546 nm between the length changes that were observed experimentally for (88 wt% Pt+12 wt% Rh) and those that were calculated from the 4th degree fitting equation (see table 4). The squares indicate data of Run No. 204; the triangles, Run No. 207. The horizontal bar centered on each point denotes the temperature interval over which the length change was measured. () encloses a data point for which the whole number of fringes was estimated. / marks a data point that was given zero weight in the fitting process. — · — · — indicates the bounds of one part per million in sample length. ····· indicates the difference between the five- and four-term fit to the experimental data.

columns 7 and 8, respectively, of table 5. The column 8 differences are plotted against the average sample temperatures in figure 6.

We recommend that eqs (16) and (17) be used to calculate the percent linear thermal expansion for (80 wt% Pt+20 wt% Rh) for reference temperatures of 0 °C and 293 K, respectively.

$$\begin{aligned}
 100 \epsilon(t, 0^\circ\text{C}) &= 100 \sum_{n=1}^4 [A_n / N(0^\circ\text{C})] t^n \\
 &= 8.674 \times 10^{-4} t + 2.538 \times 10^{-7} t^2 \\
 &\quad - 2.081 \times 10^{-10} t^3 \\
 &\quad + 1.480 \times 10^{-13} t^4
 \end{aligned} \tag{16}$$

where $N(0^\circ\text{C}) = 78,269.81$ fringes and

$$\begin{aligned}
 100 \epsilon(T, 293 \text{ K}) &= -1.731 \times 10^{-2} \\
 &\quad + 8.672 \times 10^{-4} (T - 273.15) \\
 &\quad + 2.538 \times 10^{-7} (T - 273.15)^2 \\
 &\quad - 2.080 \times 10^{-10} (T - 273.15)^3 \\
 &\quad + 1.480 \times 10^{-13} (T - 273.15)^4.
 \end{aligned} \tag{17}$$

3.4 Effect of Alloying Upon the Thermal Expansion of Pt

It is interesting to compare the temperature dependencies of the thermal expansion of the three samples studied in the course of this investigation to illustrate the effect of alloying pure platinum with rhodium.

Table 5. Experimental data for (80 wt% Pt+20 wt% Rh).

$$N(21\text{ }^{\circ}\text{C})=78,284.15\pm 0.4\text{ fringes}$$

1	2	3	4	5	6	7	8
Point No.	$t(68),\text{ }^{\circ}\text{C}$	F.F. ^a	Gas Pressure kPa	F.F. corr	$\Delta N_{\text{expt}}^{\text{b}}$	$\Delta N_{\text{calc}}^{\text{c}}$	Dev,fr ^f
Run 208							
1	231.678	.371	0.27	.367			
1a					-38.246	-38.335	.089
2	180.153	.126	0.27	.121			
2a					(82.564) ^c	82.515	.049
3	290.002	.691	0.40	.685			
3a					-39.862	-39.808	-.054
4	237.498	.830	0.47	.823			
4a					(-80.325)	-80.288	-.037
5	128.691	.502	0.20	.498			
5a					-31.865	-31.891	.026
6	84.160	.639	0.27	.633			
6a					125.772	125.762	.010
7	255.511	.409	0.27	.405			
7a					(-199.679)	-199.723	.044
8	-23.001	.735	0.27	.726			
8a					3.779	3.784	-.005
9	-17.359	.513	0.27	.505			
9a					(-0.013) ^d	-0.009	-.004
10	-17.372	.500	0.27	.492			
10a					3.980	3.936	.044
11	-11.524	.480	0.27	.472			
11a					3.243	3.246	-.003
12	-6.717	.723	0.27	.715			
12a					(0.011) ^d	.080	-.069
13	-6.599	.734	0.27	.726			
13a					5.691	5.695	-.004
14	1.802	.425	0.27	.417			
14a					6.902	6.880	.022
15	11.896	.327	0.27	.319			
15a					9.869	9.857	.012
16	26.258	.195	0.27	.188			
16a					(0.337) ^d	0.355	.018
17	26.773	.536	0.40	.525			
17a					16.906	16.799	.107
18	50.993	.438	0.27	.431			
18a					45.797	45.727	.070
19	115.513	.234	0.27	.228			
19a					46.184	46.160	.024
20	178.903	.417	0.27	.412			
20a					44.227	44.256	-.029
21	238.332	.645	0.40	.639			
21a					46.778	46.841	-.063
22	300.008	.423	0.40	.417			
22a					40.151	40.153	-.002
23	351.982	.573	0.40	.568			
23a					81.957	81.955	.002
24	455.685	.529	0.40	.525			
24a					36.923	36.897	.026
25	501.350	.454	0.53	.448			
25a					39.649	39.668	-.019
26	549.719	.102	0.53	.097			

^a F.F.; fractional fringe count at the fiducial mark.

^b ΔN_{expt} ; corrected differences in sample length, expressed in fringes.

^c Use of parentheses indicates that the integral number of fringes passing the fiducial mark during a particular temperature change was obtained from a trial plot of $\Delta N/\Delta t$ vs the mean temperature of the interval (see section 2.7).

^d Data points 9a, 12a, and 16a were given zero weight in the fitting procedure.

^e ΔN_{calc} ; fringe differences calculated for the end-point temperatures given in column 2, using eq (8) with the coefficients given in table 6.

^f Dev; $\Delta N_{\text{expt}} - \Delta N_{\text{calc}}$. These differences are plotted against the average experimental end-point temperatures in figure 6.

In table 7, we present values for the percent linear thermal expansion, $100 \epsilon(t, 0^\circ\text{C})$, for each of the three samples. These values were calculated using eqs (12), (14), and (16).

The differences between the values of the thermal expansion for the two alloys and those for pure platinum are plotted against temperature in figure 7.

Substitution of rhodium into the platinum lattice progressively reduces the thermal expansion in the temperature range 0°C to 350°C , then causes it to increase. This effect is made more noticeable as one examines the coefficient of thermal expansion. Values of this quantity are presented in table 8. The values were obtained by differentiating eqs (12), (14), and (16).

The values for the coefficient of linear thermal expansion are plotted against Celsius temperature

Table 6. Fitting parameters for the thermal expansion of (80 wt% Pt+20 wt% Rh).

Equation used in least-squares fitting procedure:

$$\Delta N(t_i, t_{i+1}) = \sum_{n=1}^m A_n (t_i^n - t_{i+1}^n) \quad (8)$$

Determination of number of polynomial terms m for "best fit":

$p=22$ data points

m	σ^a	F_m^b	$F_{0.95}(1, p-m)$
1	2.216 8	—	—
2	0.176 0	3783.4	4.35
3	0.087 1	72.0	4.38
4	0.048 6	49.6	4.41
5	0.048 9	0.8	4.45
6	0.049 6	0.2	4.49

Coefficients of 4th degree polynomial:

n	A_n	σ of A_n
1	0.678 897 5	0.000 717 2
2	0.000 198 688	0.000 006 056
3	-0.000 000 162 865	0.000 000 018 387
4	0.000 000 000 115 879	0.000 000 000 017 668

$N(0^\circ\text{C})=78,269.81$ fringes [from eq (9)]

^a σ ; the estimated standard deviation of the fit.

^b F_m ; an index used to estimate the level of significance of the m th coefficient in the equation fitted to the data.

$$F_m = 1 + (p - m + 1) \left[\left(\frac{\sigma_{m-1}}{\sigma_m} \right)^2 - 1 \right]$$

where p is the number of data points and m is the number of coefficients in the polynomial. The coefficient A_m is considered significant at the desired level of confidence if F_m is greater than the corresponding value given in the fourth column. (Entries in column 4 were taken from a standard table for the F -distribution, e.g., table III of [22].)

in figure 8. The curves show the initial reduction of the coefficient at 0°C , and the progressive increase at higher temperatures in the range that was studied in this investigation.

Table 7. Values of the percent linear thermal expansion relative to 0°C for 100% Pt and alloys of (88 wt% Pt+12 wt% Rh) and (80 wt% Pt+20 wt% Rh) calculated from eqs (12), (14), and (16), respectively.

t $^\circ\text{C}$	$100 \epsilon(t, 0^\circ\text{C}) = 100 [L(t)/L(0^\circ\text{C}) - 1]$		
	100% Pt Eq (12)	88 wt% Pt+ 12 wt% Rh Eq (14)	80 wt% Pt+ 20 wt% Rh Eq (16)
-20	-0.0177	-0.0174	-0.0172
0	0	0	0
20	0.0178	0.0176	0.0174
50	0.0447	0.0443	0.0440
100	0.0903	0.0896	0.0891
150	0.1365	0.1358	0.1352
200	0.1835	0.1827	0.1822
250	0.2311	0.2304	0.2300
300	0.2793	0.2788	0.2786
350	0.3282	0.3279	0.3280
400	0.3776	0.3777	0.3780
450	0.4277	0.4282	0.4288
500	0.4784	0.4793	0.4804
550	0.5298	0.5313	0.5328

Table 8. Values of the coefficient of linear thermal expansion for 100% Pt and alloys of (88 wt% Pt+12 wt% Rh) and (80 wt% Pt+20 wt% Rh) calculated from the temperature derivatives of eqs (12), (14), and (16), respectively.

t $^\circ\text{C}$	$10^6 \alpha(t, 0^\circ\text{C}) = 10^6 dL(t)/dt / L(0^\circ\text{C})$		
	100% Pt (d/dt)Eq (12)	88 wt% Pt+ 12 wt% Rh (d/dt)Eq (14)	80 wt% Pt+ 20 wt% Rh (d/dt)Eq (16)
$^\circ\text{C}$	$^\circ\text{C}^{-1}$	$^\circ\text{C}^{-1}$	$^\circ\text{C}^{-1}$
-20	8.790	8.677	8.570
0	8.862	8.763	8.674
20	8.931	8.846	8.773
50	9.029	8.964	8.913
100	9.183	9.147	9.125
150	9.324	9.314	9.315
200	9.457	9.468	9.487
250	9.583	9.613	9.645
300	9.705	9.752	9.795
350	9.826	9.888	9.940
400	9.949	10.023	10.085
450	10.076	10.162	10.234
500	10.210	10.306	10.392
550	10.354	10.460	10.563

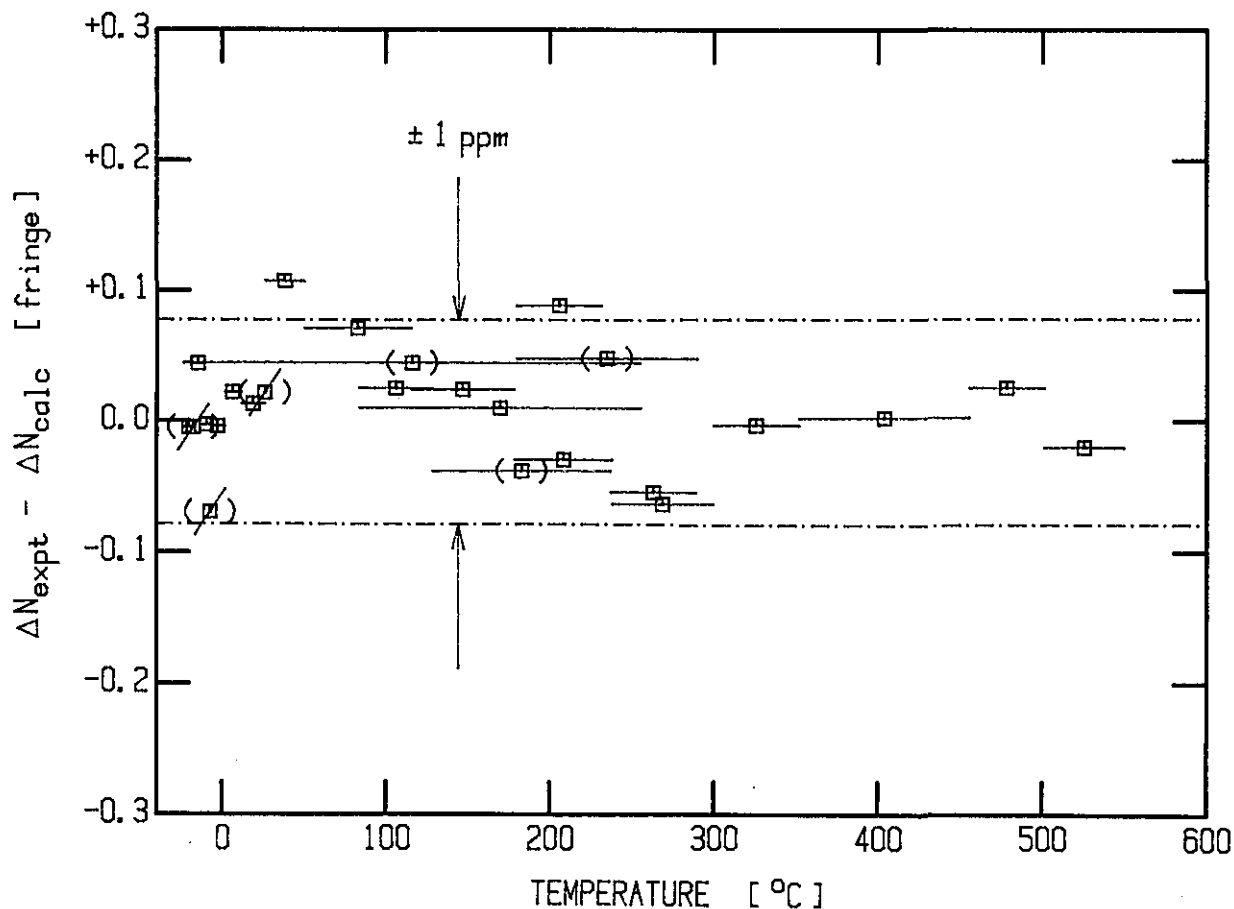


Figure 6—Differences in fringes of light at 546 nm between the length changes that were observed experimentally for (80 wt% Pt+20 wt% Rh) and those that were calculated from the 4th degree fitting equation (see table 6). The horizontal bar centered on each point denotes the temperature interval over which the length change was measured. () encloses a data point for which the whole number of fringes was estimated. / marks a data point that was given zero weight in the fitting process. — · — · — indicates the bounds of one part per million in sample length.

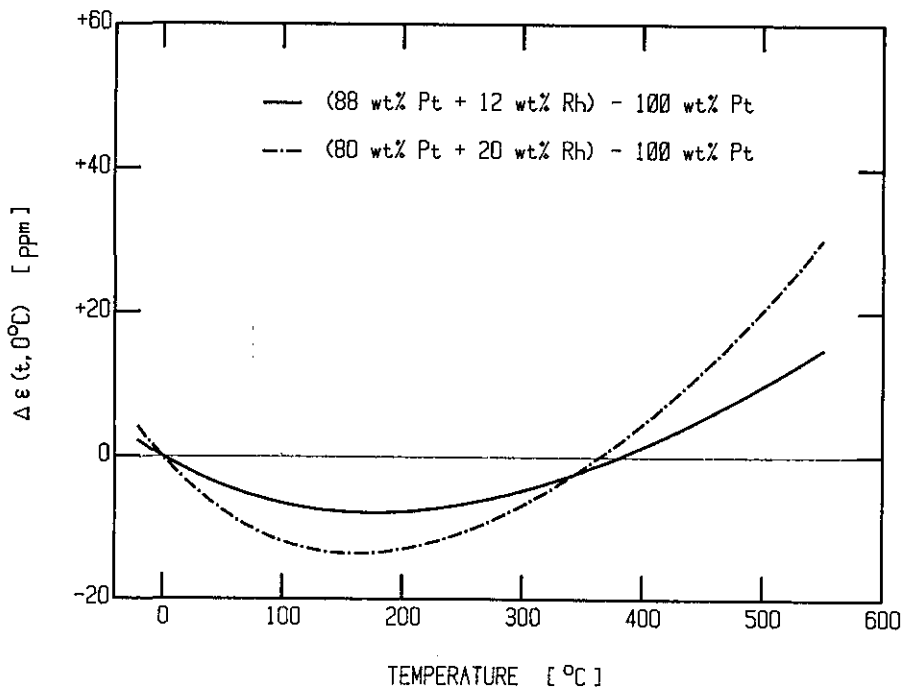


Figure 7—Differences in linear thermal expansion, $\epsilon(t, 0^\circ\text{C})$ between the (88 wt% Pt+12 wt% Rh) or the (80 wt% Pt+20 wt% Rh) sample and the 100% Pt sample, as calculated from the respective fitting eqs (14), (16), and (12).

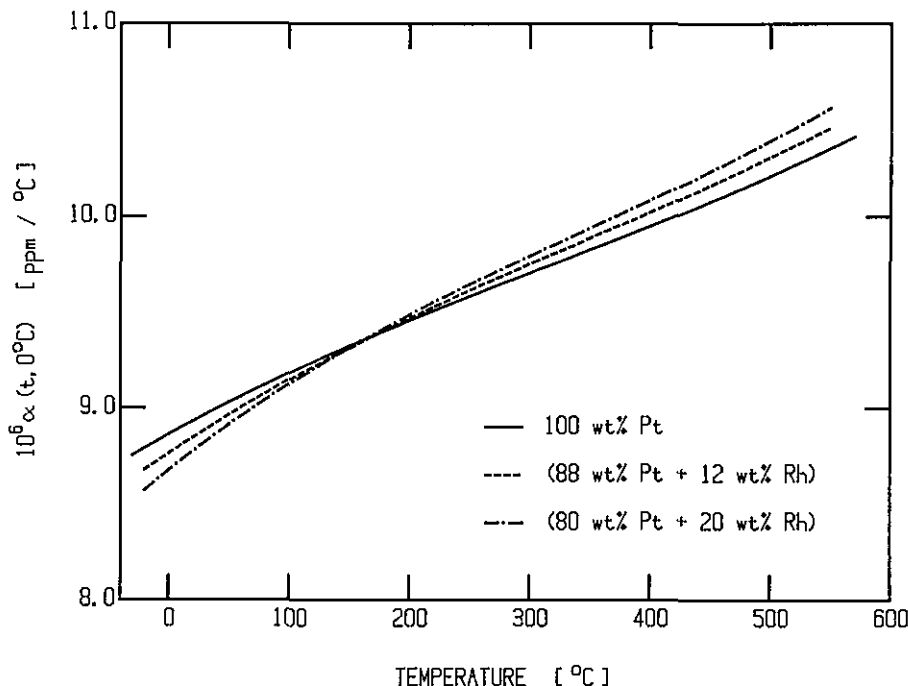


Figure 8—Coefficient of linear thermal expansion $\alpha(t, 0^\circ\text{C})$ for 100% Pt, for (88 wt% Pt + 12 wt% Rh), and for (80 wt% Pt + 20 wt% Rh). The curves were obtained by differentiating, respectively, eqs (12), (14), and (16).

4. Measurement Uncertainties

4.1 Random Uncertainties

The Merritt-Saunders method for the determination of the thermal expansion appears to provide length measurements with an overall uncertainty of 0.1 fringe or less, a value that corresponds to about 1 ppm of our sample length. The level of our overall experimental imprecision is made clear by the process of fitting the thermal expansion data for each sample (tables 2, 4, and 6) with a simple power series. Although the resolution of the fringe-counting procedure is ± 0.001 fringe, we estimate that the imprecision involved in the use of the microdensitometer to determine the fractional fringe count (col. 3 of tables 1, 3, and 5) may be 10 times as great. The determination of temperature was accomplished with relatively good precision; the thermometer sensor/bridge system used in this work allowed us to resolve temperature within $\pm 0.001^\circ\text{C}$ throughout the range of the measurements.

Another possible source of random error in our experiment is the occurrence of undetected mechanical disturbances of the apparatus during the several weeks required for the measurements. Such disturbances might lead to small displacements of the optical system and thus to incorrect values of the sample length changes.

4.2 Systematic Uncertainties

There are several potential sources of systematic error in this experiment. The fact that the uncertainties attached to predicted data points in the fitting procedures are relatively large compared to the resolution of the sample length and of the sample temperature, as we noted above, must be ascribed either to the random disturbances mentioned above or to the presence of one or more systematic errors.

Effects contributing to systematic error in the measured sample temperature include the following:

- Self-heating of the platinum resistance thermometer;
- Inadequate thermal tempering of the PRT;
- Drift in the calibration of the PRT or of the bridge that was used in its measurement;
- Temperature gradients within the sample block;
- Deviation of the sample temperature from the block temperature, arising from convective or radiative effects within the sample chamber.

Efforts were undertaken to assign limits to all of the errors listed above, either on the basis of calculations or on the basis of separate experiments conducted during this study. What follows is our estimate of these limits:

- Self-heating. We used a measuring current of 1 mA through our PRT (2.5 ohms at 0°C). In no

case did the temperature error due to self-heating exceed $0.0002\text{ }^{\circ}\text{C}$.

b) Quality of thermal tempering of the PRT. This problem caused considerable concern in the planning stage of the experiment. To help evaluate the thermal tempering, we installed a special heater—a helical coil about 6 cm long—on the guide tube that receives the PRT where it intersects shell I1. Introduction of moderate power to this heater had no discernible effect upon the measured temperature of the thermometer, leading us to conclude that the thermometer tempering was adequate.

c) Thermometer or bridge calibration drift. Periodic measurement of a standard resistor allowed us to conclude that the temperature error due to drift in calibration of the resistance bridge did not exceed $0.0001\text{ }^{\circ}\text{C}$, a negligible level. Similarly, periodic re-calibration of the PRT showed it to be stable within $0.001\text{ }^{\circ}\text{C}$.

d) Temperature gradients in the sample block. A scan was made of the vertical gradient in the sample block (I3 in fig. 1) by withdrawing the thermometer 1 cm at a time through its static seal. To do this it was necessary to maintain a pressure of 101 kPa pressure of helium gas in the apparatus. The maximum gradient observed under these conditions was $0.02\text{ }^{\circ}\text{C}/\text{cm}$. Under the usual measuring conditions, wherein the gas pressure did not exceed 1.5 kPa, we estimate the thermal gradient as less than $0.001\text{ }^{\circ}\text{C}/\text{cm}$.

e) Sample gradients arising from convective or radiative effects. Heat transfer calculations indicate that the temperature difference between the sample and its enclosure arising from convective or radiative effects did not exceed $0.001\text{ }^{\circ}\text{C}$. No experimental verification of this result was attempted.

Another systematic error in the Merritt-Saunders experiment can arise from differences in the thermal expansions of the sample and of the glass plates that touch it. It is likely that the contact between the glass plates A and B and the sample pads a-a, b-b, and c-c takes place at different points during the measurement process. Given the thermal expansion rates of the two materials and the sample geometry, one can expect the relative separation of the points of contact on each plate to change by about $6.5\text{ }\mu\text{m}$ as the system temperature varies from $-20\text{ }^{\circ}\text{C}$ to $560\text{ }^{\circ}\text{C}$. While this motion corresponds to a change in angle of the upper plate of only 2.5 microdegrees and thus to a shift in the fringe count at the fiducial mark of only 0.002 fringe, if the motion were to take place in a hysteretic and erratic fashion, then the fringe pattern could be disturbed to a larger extent.

Systematic errors can arise from incorrect measurement of the filling-gas pressure or from outgassing within the sample chamber during the measurements, from incorrect evaluation of the wavelength of the radiation used to form the fringe pattern, from use of incorrect values of the refractive index of the filling gas as given by eq (3), and from variation in developing or handling the film. All of these would appear to be relatively small with respect to the imprecision found in the fitting procedure. The uncertainty in the determination of the reference lengths of the samples is 30 ppm, approximately 10 ppm of that quantity arising from uncertainty in the reading of the dial micrometer and 20 ppm owing to uncertainty in the temperature of the samples and gage blocks; an overall bias in the sample length at this level, however, has only a negligible effect on the calculated values of the thermal expansion.

Yet another systematic error can arise from changes in the sample properties during the measurements. Barter and Darling [23] have illustrated the drift in the thermal expansion of an (80 wt% Pt+20 wt% Rh) sample that accompanies the first heating of a hard-drawn material to its annealing temperature. Hahn and Kirby [24], on the other hand, have reported that subsequent measurements of annealed samples of Pt showed no perceptible drift in the thermal expansion. We took care to anneal our samples prior to measurement, so that we expect only negligible error from this source.

In table 9, we summarize our estimates of the uncertainties arising in the present experiment.

Table 9. Uncertainties in Merritt-Saunders thermal expansion measurements.

A. Random

1. Overall experimental uncertainty (from fitting procedure) < 1 ppm of sample length.
2. Uncertainty of fringe measurement ± 0.01 fringes.
3. Sample temperature resolution $\pm 0.001\text{ }^{\circ}\text{C}$.
4. Mechanical shock to optical system during measurement—unknown magnitude.

B. Systematic

1. Sample temperature different from measured temperature $< 0.001\text{ }^{\circ}\text{C}$.
2. Fringe count error— < 0.01 fringe.
3. Refractive index of medium incorrect— < 0.02 fringe.
4. Error in interferometer wavelength— < 1 ppm.
5. Film and reader irregularities—negligible.
6. Sample property changes during measurements—unknown.

5. Comparison With Other Results

High-purity platinum serves as a standard for thermal expansion measurements. Therefore it seems very useful to compare high-precision measurements on this material that originate in different laboratories.

Numerous workers have studied the thermal expansion of Pt and Pt-Rh alloys. Nearly all of the results published prior to 1975 have been compiled by Kirby and others in the form of graphs and tables of coefficient of linear thermal expansion, $\alpha(T, 293 \text{ K}) = [1/L(293 \text{ K})] [dL(T)/dT]$, and percent linear thermal expansion relative to 293 K, $100 \epsilon(T, 293 \text{ K}) = 100 [L(T) - L(293 \text{ K})]/[L(293 \text{ K})]$ [4].

In analyzing our data, we have attempted to use the most direct fitting process available, that is, one in which the experimentally determined sample length changes were fitted by a polynomial consisting of differences of increasing powers of the endpoint temperatures [eq (8)]. By applying the F-test for evaluating the significance of the coefficients, we attempted to avoid problems that can arise from "over-fitting" experimental data (i.e., using polynomial functions of higher degree than justified by the precision of the data).

We remind the reader that a wide variation exists in the manner of expression of thermal expansion results, and that careless use of these expressions can lead to discrepancies among similar data [25]. Any of the customary forms for the expression of thermal expansion that are found in the literature, including

$$\frac{L(t) - L(t_{\text{ref}})}{L(t_{\text{ref}})(t - t_{\text{ref}})} \quad (\text{"average thermal expansivity"})$$

$$\frac{L(t + dt) - L(t - dt)}{L(t_{\text{ref}}) 2 dt} \quad (\text{"thermal expansivity"})$$

$$\frac{L(t + dt) - L(t - dt)}{L(t) 2 dt} \quad (\text{"instantaneous thermal expansivity"})$$

$$\frac{L(t)}{L(t_{\text{ref}})} \quad (\text{"linear thermal expansion"})$$

$$\frac{100 [L(t) - L(t_{\text{ref}})]}{L(t_{\text{ref}})} \quad (\text{"percent linear thermal expansion"})$$

can be derived directly from fitting equations such as eq (8).

5.1 100% Pt

Twenty-eight sets of data for the linear thermal expansion of 100% Pt have been critically analyzed by the Thermophysical Properties Research Center (TPRC) with the result that a "recommended curve" for the percent linear thermal expansion over the range 293 K to 1900 K has been offered [5]

$$100 \epsilon(T, 293 \text{ K}) = 9.122 \times 10^{-4} (T - 293) + 7.467 \times 10^{-8} (T - 293)^2 + 4.258 \times 10^{-11} (T - 293)^3. \quad (18)$$

Note that temperature in eq (18) is expressed in kelvins; we denote these temperatures by T . At selected temperatures TPRC also tabulated "recommended values" for this quantity which differ slightly from those given by eq (18).

The recent study by Hahn and Kirby [24] and the older work by Holborn and Day [26] most nearly approximate our own work in experimental technique, temperature range, and precision. Hahn and Kirby represented their results for the percent linear thermal expansion of 100% Pt for the temperature range 293 to 1900 K by the relation

$$100 \epsilon(T, 293 \text{ K}) = 0.2279 + 6.117 \times 10^{-4} T + 8.251 \times 10^{-7} T^2 - 1.1187 \times 10^{-9} T^3 + 9.1523 \times 10^{-13} T^4 - 3.6754 \times 10^{-16} T^5 + 5.893 \times 10^{-20} T^6. \quad (19)$$

Holborn and Day expressed their results as an equation in degrees Celsius for the coefficient of linear thermal expansion. Their integrated equation referenced to 293 K is

$$100 \epsilon(T, 293 \text{ K}) = -0.0176 + 8.866 \times 10^{-4} \times (T - 273.15) + 1.322 \times 10^{-7} \times (T - 273.15)^2. \quad (20)$$

In table 10, values of the percent linear expansion relative to 293 K as calculated from eqs (18) to (20) plus TPRC recommended values for specific temperatures are compared to values calculated

Table 10. Values of the percent linear thermal expansion relative to 293 K for 100% Pt from various selected sources.

T		$100 \epsilon(T, 293 \text{ K}) = 100 [L(T)/L(293 \text{ K}) - 1]$			
K	This work Eq (12)	TPRC [5] recommended value Eq (18)	Hahn and Kirby [24] Eq (19)	Holborn and Day [26] Eq (20)	
273.15	-0.0177				-0.0177
293	0	0	0	0	0
300	0.0063	0.0064	0.0062	0.0062	0.0062
400	0.0974	0.096	0.0985	0.0971	0.0969
500	0.1913	0.189	0.1924	0.1910	0.1903
600	0.2878	0.288	0.2883	0.2873	0.2863
700	0.3867	0.388	0.3865	0.3858	0.3849
800	0.4881	0.490	0.4872	0.4866	0.4862

from eq (13). Curves showing the differences between eqs (18) to (20) and our values are plotted against degrees Celsius in figure 9. The differences are generally larger than the total uncertainty in our values which we believe to be less than 1 ppm.

5.2 (88 wt% Pt+12 wt% Rh) Alloy

No other thermal expansion data were found for the (88 wt% Pt+12 wt% Rh) alloy. Ebert [28] has published values for the thermal expansion relative to 0 °C of pure Rh which indicate an uncertainty of about 10 ppm. Using the Ebert data combined with

our values for 100% Pt we have estimated the thermal expansion of the (88 wt% Pt+12 wt% Rh) alloy as

$$\epsilon(t, 0 \text{ }^\circ\text{C})_{\text{Pt}(1-x)\text{-Rh}_x} = (1-x) \epsilon(t, 0 \text{ }^\circ\text{C})_{\text{Pt}} + x \epsilon(t, 0 \text{ }^\circ\text{C})_{\text{Rh}} \quad (21)$$

where $x=0.12$. The resulting values are given in table 11 together with those for 100% Pt given by eq (12) and for 100% Rh as reported by Ebert. The values for the thermal expansion of alloy as estimated in this manner are all within 10 ppm of our results.

Table 11. Values of the percent linear thermal expansion relative to 0 °C for the (88 wt% Pt+12 wt% Rh) alloy [eq (14)] compared with those estimated using eq (21) with $x=0.12$.

t		$100 \epsilon(t, 0 \text{ }^\circ\text{C}) = 100 [L(t)/L(0 \text{ }^\circ\text{C}) - 1]$		
°C	100% Pt	100% Rh	88 wt% Pt+12 wt% Rh	
	Eq (12)	[28]	This work Eq (14)	Estimated Eq (21)
0	0	0	0	0
50	0.0447	0.040	0.0443	0.0441
100	0.0903	0.085	0.0896	0.0899
200	0.1835	0.180	0.1827	0.1831
300	0.2793	0.280	0.2788	0.2794
400	0.3776	0.385	0.3777	0.3785
500	0.4784	0.490	0.4793	0.4798

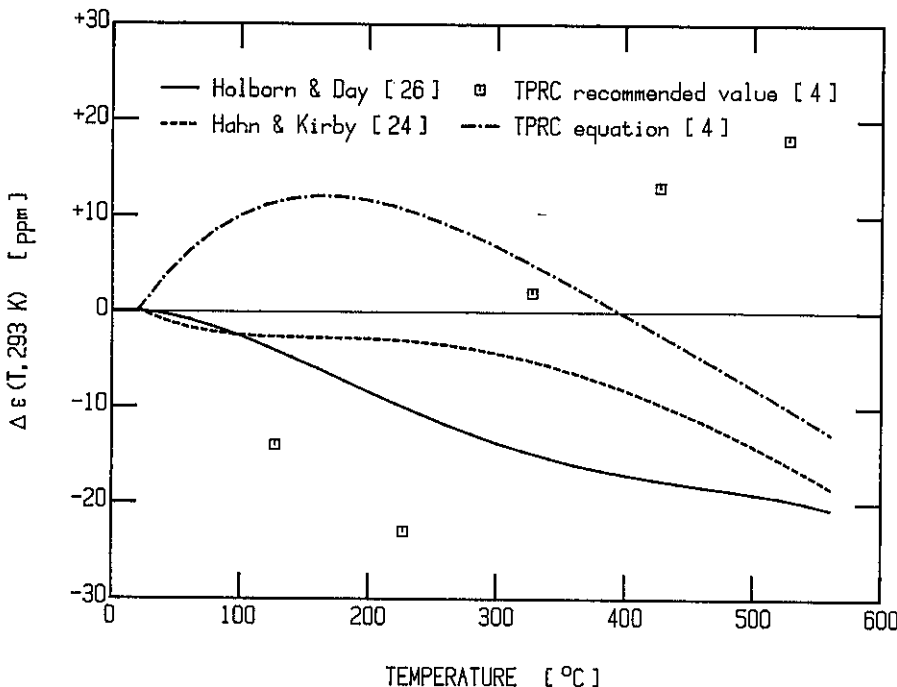


Figure 9—The differences between various published representations for the linear thermal expansion of 100% Pt and that obtained in this research.

5.3 (80 wt% Pt+20 wt% Rh) Alloy

The linear thermal expansion of the (80 wt% Pt+20 wt% Rh) alloy has also been measured by Day and Sosman [27] and by Barter and Darling [23].

Day and Sosman represented their measurements as an equation for the coefficient of linear thermal expansion referenced to 0 °C. The integral of their equation, expressed as percent linear thermal expansion is

$$100 \epsilon(t, 0 \text{ } ^\circ\text{C}) = 8.79 \times 10^{-4} t + 1.61 \times 10^{-7} t^2. \quad (22)$$

Once again we have estimated the percent linear thermal expansion of the (80 wt% Pt+20 wt% Rh) alloy using the data of Ebert for 100% Rh and our values for 100% Pt combined according to eq (21) with $x=0.20$. The resulting values are given in table 12 together with values representative of the Day and Sosman measurements as calculated by eq (22) and the results given by Barter and Darling. The relationship between these quantities is plotted against degrees Celsius in figure 10 with the smooth curve indicating the difference between eq (22) and eq (16). Note that the differences between thermal expansion values calculated from eq (16) and the results of Barter and Darling are plotted at 1/10 scale. The close agreement between the values estimated from eq (21) and our results, for both the 12% and the 20% Rh alloy, as well as the close agreement between our results and those of Day and Sosman, indicate that significant systematic error may exist in the Barter and Darling experimental results.

Table 12. Values of the percent linear thermal expansion relative to 0 °C for the (80 wt% Pt+20 wt% Rh) alloy from various sources including those estimated using eq (21) with $x=0.20$.

t °C	$100 \epsilon(t, 0 \text{ } ^\circ\text{C}) = 100 [L(t)/L(0 \text{ } ^\circ\text{C}) - 1]$			
	Day and Sosman Eq (22)	Barter and Darling [23]	This work Eq (16)	Estimated Eq (21)
0	0	0	0	0
50	0.0444		0.0440	0.0438
100	0.0895	0.063	0.0891	0.0892
200	0.1822	0.140	0.1822	0.1828
300	0.2782	0.23	0.2786	0.2795
400	0.3774	0.32	0.3780	0.3791
500	0.4798	0.43	0.4804	0.4807

6. Summary and Conclusions

In this paper, we have described in some detail our realization of the Merritt-Saunders technique for the measurement of linear thermal expansion over the temperature range $-27 \text{ } ^\circ\text{C}$ to $550 \text{ } ^\circ\text{C}$. We report measurements, using this method, made on platinum and two platinum-rhodium alloys. We believe that the equation fitted to the experimental data of each sample accurately represents its linear thermal expansion to within 1 ppm of sample length. Our data (some 86 points for three samples) show scatter from the fitting equations that is (with one exception) not larger than 2 ppm.

We have expended considerable effort to fit our data carefully and to record clearly the fitting parameters in order that the reader who may wish to utilize our results will be better able to judge their applicability. We have taken care to clearly define our terminology after noting that the clarity of thermal expansion nomenclature in the literature is not always adequate for the user's needs.

Where possible, we have compared our results with those of other experimenters. We have made these comparisons in terms of the linear thermal expansion, $\epsilon(t, t_{ref})$, even in those instances in which the authors have given an analytical representation of the experimental data in terms of the coefficient of linear thermal expansion, $\alpha(t, t_{ref})$, (e.g. Holborn and Day [26] for 100% Pt). We chose to do so because we find this form of comparison to be the most useful for our needs and anticipate that it will be the information most sought by the reader. With the exception of the data of Barter and Darling [23] for the (80 wt% Pt+20 wt% Rh) alloy, we find agreement with other results within ± 20 ppm throughout the temperature range of our experiments.

Finally, we have shown a close correspondence between the measured linear thermal expansion of two Pt-Rh alloys and values estimated by adopting a linear approximation using pure Pt and pure Rh thermal expansion data.

We are greatly indebted to L. A. Guildner for the design of the thermal expansion apparatus described herein and for his supervision of the experimental measurements.

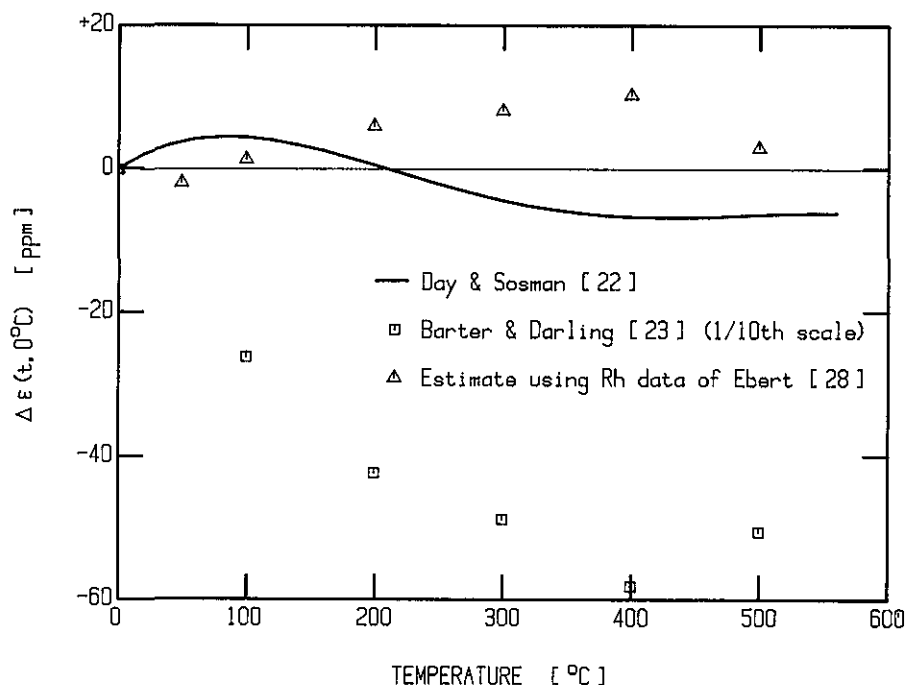


Figure 10—The differences between various published representations for the linear thermal expansion of (80 wt% Pt+20 wt% Rh) and that obtained in this research.

References

- [1] Clothier, W. K., A calculable standard of capacitance, *Metrologia* 1 36-55 (1965).
- [2] Driscoll, R. L., Measurement of a current with a Pellat-type electrodynamic meter, *J. Res. NBS* 60 287-296 (1958).
- [3] Bell, G. A., and J. B. Patterson, Density standards—the density and thermal dilatation of water, *Precision Measurement and Fundamental Constants II*, Taylor, B. N., and W. D. Phillips, eds, NBS (U.S.) Spec. Pub. 617 445-447 (1984).
- [4] Touloukian, Y. S.; R. K. Kirby, R. E. Taylor, and P. D. Desai, Thermal Expansion, *Metallic Elements and Alloys*, vol 12 in *Thermophysical Properties of Matter*, Touloukian, Y. S., and Ho, C. Y., eds, Plenum Press, New York, 1975.
- [5] MacDonald R. A., and W. M. MacDonald, Thermodynamic properties of fcc metals at high temperatures, *Phys. Rev. B* 24 1715-1724 (1981).
- [6] Collins J. G., and G. K. White, Thermal expansion of solids, Ch IX in *Progress in Low Temperature Physics*, vol IV, 1964, North-Holland Pub. Co., Amsterdam, pp. 450-479.
- [7] Yates, B., *Thermal Expansion*, Plenum Press, New York, 1972, 121 pp.
- [8] Waterhouse, N., and B. Yates, The interferometric measurement of the thermal expansion of silver and palladium at low temperatures, *Cryogenics* 8 267-271 (1968).
- [9] Andres, K., The measurement of thermal expansion of metals at low temperatures, *Cryogenics* 2 93-97 (1961).
- [10] Shapiro, J. M.; D. R. Taylor, and G. M. Graham, A sensitive dilatometer for use at low temperatures, *Can. J. Phys.* 42 835-847 (1964).
- [11] Batchelder, D. N., and R. O. Simmons, X-ray lattice constants of crystals by a rotating-camera method: Al, Ar, Au, CaF₂, Cu, Ge, Ne, Si, *J. Appl. Phys.* 36 2864-2868 (1965).
- [12] White, G. K., Measurement of thermal expansion at low temperatures, *Cryogenics* 1 151-158 (1961).
- [13] Carr, R. H., and C. A. Swenson, Application of a variable transformer to the study of low temperature thermal expansion, *Cryogenics* 4 76-82 (1964).
- [14] Commercially available products are identified herein only for the sake of accurate description. No implication is intended that these items are superior to others of the same type, or that the NBS endorses the use of these products.
- [15] Candler, C., *Modern Interferometers*, Hilger & Watts, Ltd., 1951, Ch IV.
- [16] Merritt, G. E., Application of the interferometer to measurements of the thermal dilatation of ceramic materials, *Scientific Papers of the Bureau of Standards* 19 No. 485 (1924).
- [17] Saunders, J. B., An apparatus for photographing interference phenomena, NBS Research Paper RP1668, *J. Res. NBS* 35 157-186 (1945).
- [18] The International Practical Temperature Scale of 1968; amended Edition of 1975, *Metrologia* 12 7-17 (1976).
- [19] Cutkosky, R. D., An a-c resistance thermometer bridge, *J. Res. NBS* 74c 15-18 (1970).
- [20] Kaufman, V. Wavelengths, energy levels, and pressure shifts in mercury 198, *J. Opt. Soc. Am.* 52 866-870 (1962).
- [21] See, for example, *American Inst. of Physics Handbook*, 3rd Ed., Gam, D. E., ed, McGraw-Hill Book Co., New York, 1972, Ch 6.
- [22] Mandel, J., *The Statistical Analysis of Experimental Data*, Wiley & Sons, New York (1964) Ch 8.
- [23] Barter, B., and A. S. Darling, Thermal expansion of rhodium-platinum alloys, *Platinum Metals Rev.* 4 138-140 (1960).
- [24] Hahn, T. A., and R. K. Kirby, Thermal expansion of platinum from 293 to 1900 K, in *Thermal Expansion—1971*, Graham, M. G., and H. E. Hagy, eds; Amer. Inst. of Phys. Conf. Proc. #3, Wolfe, H. C., Series ed, Amer. Inst. of Phys., New York, 1972, pp. 87-95.

- [25] MacDonald, R. A., The thermal expansion coefficient of fcc metals, in Thermal Expansion 8, the Proceedings of the 8th International Thermal Expansion Symposium, Gaithersburg, Maryland, 1981, Plenum Press, New York, 1984, pp. 11-19.
- [26] Holborn, L., and A. L. Day, On the expansion of certain metals at high temperatures, Amer. J. Sci., 4th Series **11** 374-390 (1901).
- [27] Day, A. L., and R. B. Sosman, The nitrogen thermometer from zinc to palladium, Amer. J. Sci., 4th Series **29** 93-161 (1910).
- [28] Ebert H., Bestimmung der Wärmeausdehnung von einigen aluminium- und magnesium-legierungen, sowie vom rhodium, Phys. Zeit. **39** 6-9 (1938).

News Briefs and Reports

New Technical Developments

PERFORMANCE MEASUREMENT OF MULTIPROCESSOR COMPUTERS: INITIAL PROGRESS

NBS has undertaken a project to improve the quantification of the performance of multiprocessor computers. Much of this work will apply to conventional computers as well. Computer performance measurement is seen as involving (1) an understood stimulus, the test (benchmark) programs run to test the computer; (2) techniques for attaching to the multiprocessor computer to capture its response; and (3) techniques for analyzing the response for the aid of designers and users.

The provision of test programs has taken two paths: the identification and collection of existing benchmark programs, and the creation of small test routines designed to elucidate specific aspects of performance. This growing collection of benchmark programs is now available on-line through the DARPA internet by sending mail to <nbslib@icstcmr.arpa>. If sent the message "send index," the automated mail system will return additional instructions on how to get the desired programs. The mail system was kindly supplied by Dr. J. Dongarra of the Argonne National Laboratory.

A review of techniques for capturing the response of the system under test has been reported in an NBS Interagency Report [1]. The discussion of the various parameters that could be measured estimates both their usefulness and the difficulty of measuring them. A very simple Interim Measurement System has been applied to a testbed shared-memory multiprocessor to capture detailed execution-duration measurement of short sequences of instructions with insignificant perturba-

tion of the execution. A much more complete set of measurement hardware is under construction.

The analysis and presentation of the results of measurement are critical to its utility. The results from test programs which were run must be weighted to predict performance of the machine (architecture) under test on the algorithm (application) proposed. The designer who will improve computer hardware or system software needs information presented differently from that required by the programmer trying to improve the performance of a specific application.

For further information contact Robert J. Carpenter, National Bureau of Standards, Gaithersburg, MD 20899.

Reference

- [1] Roberts, J.W., Performance Measurement Techniques for Multiprocessor Computers, NBSIR 85-3296 (1985).

GRAPHICS STANDARD APPROVED

The Secretary of Commerce has approved a standard [1] for the Federal government which specifies a library (or toolbox package) of subroutines for producing and manipulating two-dimensional pictures. The standard will make it easier to transfer graphics application programs among different computers and graphics devices. It adopts a voluntary industry standard (ANSI X3.124.1985) which NBS helped develop.

Reference

- [1] Federal Information Processing Standard (FIPS) 120, Graphical Kernel System, National Technical Information Service, Springfield, VA 22161 (\$35.50 prepaid).

NONDESTRUCTIVE ULTRASONIC METHOD DETECTS FLAWS IN CERAMIC POWDERS

A new ultrasonic method for detecting flaws in compacted ceramic powders has been developed at

NBS. It is the first nondestructive evaluation technique to permit ceramic producers to fully automate the inspection of compacted powders while the material is in the mold.

The NBS system provides producers with information on the uniformity and density of materials at almost any stage of compaction. It will help manufacturers screen out defective parts before costly processing takes place.

The ultrasonic sensor method, which provides a way to "dry" couple a transducer to a green-state (unfired) ceramic without contaminating the material, was developed at the Bureau by a Johns Hopkins University materials science graduate student and an NBS physicist. They modified a commercial steel mold by placing a piezoelectric transducer on the compaction shaft. The transducer generates an ultrasonic wave down into the mold where some of it is transmitted into the ceramic powder and some is reflected back towards the transducer. The ultrasonic echoes are recorded as they reflect up and down through the sample until the pulse dies out.

Measurement of the time between pulses at the top and bottom of the mold permits calculation of the velocity of sound in the ceramic powder. Since the velocity depends on the consistency of the unfired material, this information can be used by producers to improve the compaction process.

The technique can be a complementary and effective quality control tool when it is combined in a feedback loop with other in-line sensors such as those used to measure temperature, pressure, and humidity, according to the scientists.

The system can perform both compressional and shear wave measurements in ceramic powders. The resulting data can provide information on the porosity of the material and permit producers to measure how well organic binders are working. Binders are typically used to coat and lubricate ceramic particles so that they more readily slide by each other during compaction in order to form a high density compact.

The new ultrasonic sensor method has been developed as a part of the NBS effort to apply nondestructive evaluation techniques to measure the properties and characteristics of materials for in-line monitoring and process control during manufacturing.

For further information, contact Gerald V. Blessing, National Bureau of Standards, Gaithersburg, MD 20899.

SYNCHROTRON RADIATION OFFERS RESEARCHERS NEW TOOL

NBS has completed the first year of experimental operations and instrument evaluations on the materials science x-ray beamline at the National Synchrotron Light Source in Brookhaven, NY. The beamline offers materials scientists from government, industry, and universities a research tool combining the highest brightness, lowest emittance source for x rays in the world with high-resolution x-ray optics for use in characterizing the microstructures of materials. It enables researchers to conduct real-time, in-situ measurements on a micron scale. With remote control instruments, scientists can observe and record microstructural changes in metal, ceramic, and polymer materials as they are exposed to different thermal, electromagnetic, or mechanical environments.

For information on using the materials science part of the NBS x-ray beamline facility, a joint effort between the Bureau and the Naval Research Laboratory, contact Dr. Gabrielle G. Long, National Bureau of Standards, Gaithersburg, MD 20899.

SILICON DIOXIDE STUDY AIMED AT ELECTRONICS, FIBER INDUSTRIES

NBS researchers, in collaboration with Professor Joseph Katz of Johns Hopkins University, are using a diffusion flame and laser diagnostic methods to examine the formation and growth of silicon dioxide particles. How those particles form is important, for example, to the optical fiber industry. There, control of the particle formation process and deposition of a uniform layer is critical in the production of high-quality optical fibers. Katz has designed and constructed a counter-flow diffusion flame burner that simulates industrial processes by forming silicon dioxide particles in a flat, highly uniform flame well suited for optical probing. Laser scattering techniques are used to determine concentration of intermediate compounds such as SiO and OH. Electron microscopy also is being used to examine particles in samples withdrawn from the flame.

For further information contact Hratch Semerjian, National Bureau of Standards, Gaithersburg, MD 20899.

New Standard Reference Data

MATERIALS AIMED AT MORE ACCURATE ALCOHOL/GASOLINE BLENDS

Four standard reference materials now available from NBS will help laboratories maintain measurement accuracy when blending various alcohols—methanol, ethanol, and t-butanol—with automotive fuels. Blending is on the upswing because of regulatory decreases in amounts of lead allowed per fuel gallon. Alcohol, like lead, can be used to boost gasoline octane. The new SRMs provide reference standards for checking the accuracy of laboratory instruments and evaluating analytical methods.

The reference materials, which are certified accurate in their alcohol content, are as follows: SRM 1837—Methanol (9 percent by volume) and t-Butanol (6 percent) in Reference Fuel; SRM 1838—Ethanol (10 percent) in Reference Fuel; SRM 1839—Methanol (0.3 percent) in Reference Fuel; and SRM 1829—Alcohols in Reference Fuel, which consists of all three alcohols. The reference fuel is 90-octane gasoline. SRMs 1837, 1838, and 1839 each have five sealed glass vials of material, while SRM 1829 consists of two vials of each of the three alcohols. These SRMs cost \$92 apiece.

New Services From NBS

NEW NBS FACILITY EYED AS IMPROVEMENT TO FLOW CALIBRATIONS

Flow Technology, Inc., a flow measurement instrument manufacturer, has donated a fluid meter calibration facility to NBS which officials anticipate will significantly expand the Bureau's flow rate calibration capabilities. The facility is valuable for checking, for instance, the operation of turbine meters the aircraft industry uses to determine engine performance. The new capability will supplement an existing facility donated to NBS by the Navy Department 30 years ago and used since to perform flow meter calibrations. NBS researchers say the new device has improved features such as high-speed data processing, efficient change of fluids, and more rapid overall performance. It also allows expansion into calibration ranges previously not covered. Because the device is more efficient

than its predecessor, in-house savings will be passed on to calibration customers.

For further information, contact George Mattingly, National Bureau of Standards, Gaithersburg, MD 20899.

NBS AND HEALTH PHYSICS SOCIETY LAUNCH NEW PROGRAM FOR RADIATION INSTRUMENT CALIBRATION

NBS and the Health Physics Society have begun a new national program to accredit laboratories that calibrate instruments used to measure ionizing radiation.

NBS will continue to be the primary standards lab for these instruments, such as Geiger counters, which are regularly used in industry to protect radiation workers by making on-the-spot measurements of radiation levels. The Society will provide a new service to accredit secondary- and tertiary-level calibration laboratories using procedures and technical criteria developed by the Society in cooperation with the NBS Office of Radiation Measurements.

The Health Physics Society is a national organization of professionals in occupational radiation protection dedicated to improving the standards and performance of their profession.

The new program, according to the HPS, will provide radiation protection professionals greatly expanded access, directly and indirectly, to the national standards maintained by NBS. This, says the Society, will result in improved uniformity, accuracy, and traceability of ionizing radiation measurements. There are more than 1.3 million industrial radiation workers in the United States who could be affected by the new program.

Initially, laboratories will be accredited for the calibration of x-ray and gamma-ray instruments. The program will later be extended to include beta and neutron radiation. Fees, scaled to cover the costs of the program, are expected to range between \$5,000 and \$8,000 for a 3-year secondary-level accreditation, and between \$3,000 and \$4,000 for tertiary-level accreditation.

HPS plans to accredit as many as 12 secondary laboratories, which will have their standards calibrated and performance tested by NBS, and up to 40 tertiary labs, with standards calibrated and performance tested by the secondary labs. Applications for accreditation will be accepted by HPS after January 1, 1987.

NBS has actively pursued this system of secondary calibration laboratories for radiation mea-

surements for several years to satisfy rapidly increasing demands for calibrations.

NBS currently has similar programs with the Conference of Radiation Control Program Directors, which accredits secondary-level calibration labs to serve state radiation control officers; and with the American Association of Physicists in Medicine, which accredits laboratories that calibrate instruments which in turn are used to calibrate radiation equipment in hospitals and clinics.

NBS also has set up a procedure, under its National Voluntary Laboratory Accreditation Program (NVLAP), to accredit laboratories that process the personnel dosimeters worn by radiation workers.

New Standard Reference Materials*

NBS DEMONSTRATES ADVANCES IN COMPUTERIZED DATABASES

Several new prototype databases for use with personal computers were demonstrated by NBS scientists to more than 300 data experts from the world's leading industrial nations at the 10th International CODATA (Committee on Data for Science and Technology) Conference held in Ottawa, Canada, July 1986. The demonstrations included databases on the thermophysical properties of water (steam) and of 12 different fluids. Special graphics software programs also were displayed for phase diagrams of ceramics and for diagrams on corrosion in materials.

Dr. David R. Lide, Jr., director of the NBS Office of Standard Reference Data and newly elected president of CODATA, says the international group is working to establish agreements on the format of computerized databases, including those designed for personal computers. Lide says, "Many organizations are exploring the use of magnetic and optical discs which will provide users in physics, chemistry, and other fields with an easy, portable way to access databases only available in printed form or through on-line networks."

For information on CODATA or the NBS standard reference data program, contact the Office of Standard Reference Data, National Bureau of Standards, Gaithersburg, MD 20899.

* SRMs can be ordered from the Office of Standard Reference Material, NBS, Gaithersburg, MD 20899, Telephone 301-921-2045.

Report: I-R 100 Winners

SIX NBS PROJECTS WIN 1986 I-R 100 AWARDS

Six projects in innovative instrumentation and measurement technology from NBS have been cited in the annual I-R 100 competition sponsored by *Research & Development* magazine.

I-R 100 awards are given by the magazine to honor the "100 most significant" new technical products of the preceding year. NBS has received 51 I-R 100 awards since first entering the competition in 1973.

This year, NBS research teams were cited for work on an extremely efficient spectrometer for measurements in the "soft x-ray" portion of the spectrum; for the development of a new reference standard for the U.S. volt; for the development of a new calibration tool for electrical waveform recorders; for the development of a novel reference electrode suitable for use in nonaqueous media; for the invention of an innovative new "computing engine" to process images for machine vision systems; and for the development of a new reference material for microscopic measurements, which is also the first commercial product to be made in space.

Soft X-Ray Spectrometer

A team from Oak Ridge National Laboratory, NBS, and the University of Tennessee at Knoxville won an I-R 100 award for the development of a new, extremely sensitive spectrometer for use with synchrotron radiation sources in the soft x-ray region of the spectrum.

The instrument was specially designed to measure very-low-intensity radiation with efficiencies 1,000 to 10,000 times higher than conventional spectrometers. This means that measurements can be made either with weaker sources, at much higher resolutions, or in much less time (e.g. minutes instead of days). The new spectrometer detects radiation in the range from 50 nanometers to 1.2 nm (20 eV to 1 KeV).

It is particularly well suited to studying the spectra of light elements, particularly in fragile materials such as surface layers, organic materials, and light alloys. The spectrometer is presently being used in experiments at the NBS Synchrotron Ultraviolet Radiation Facility (SURF-II) and the Brookhaven National Synchrotron Light Source (NSLS) facility.

The high-efficiency, soft x-ray spectrometer was developed by Thomas A. Callcott and King L. Tsang of the University of Tennessee at Knoxville, Edward T. Arakawa of Oak Ridge National Laboratory (Martin Marietta Energy Systems, Inc.), and David L. Ederer of NBS.

New Voltage Standard

Three NBS researchers shared an I-R 100 award for the development of a voltage reference system that gives any laboratory access to a useful voltage standard comparable in accuracy to the U.S. national standard maintained by NBS.

The U.S. standard volt is defined in terms of quantized voltages produced by a superconducting device known as a "Josephson junction." The voltage produced by a Josephson junction depends only on a fundamental constant and the frequency of a microwave field applied to the junction, thus any laboratory can produce standard voltages limited in accuracy only by the accuracy of the frequency generator, which can be quite high.

The problem has been that a single junction produces only very low levels of voltage—about five thousandths of a volt at best—which limits its usefulness to a handful of national standards laboratories. Previous attempts have been made to link several junctions together in series to produce more reasonable voltages, but technical difficulties limited these to arrays of 20 junctions or fewer.

After 10 years of effort, NBS researchers succeeded in developing an integrated circuit chip that incorporates 2,076 Josephson junctions, and that can produce any voltage between 0.1 and 1.3 volts at accuracies 10 to 100 times better than any system previously available, even at NBS.

Because the Josephson array is a direct implementation of the U.S. legal volt, it needs no calibration. The device has the potential to completely revolutionize the national system for voltage measurements.

Clark A. Hamilton, Richard L. Kautz and Frances L. Lloyd of NBS developed the Josephson series array voltage standard.

Precision Step Generator

Three NBS researchers have introduced a calibration standard for transient waveform recorders that is an improvement over existing commercial instruments in either accuracy or variability of voltage levels.

Transient waveform recorders are used to measure rapid voltage pulses in applications such as re-

search into automotive engine performance or the testing of electric power equipment for its vulnerability to lightning. These instruments also play key roles in nuclear fusion research and weapons testing.

The NBS device generates precise, fully programmable voltage steps which exhibit fast transitions and exceptionally smooth settling to the final voltage value. Two ranges, ± 5 V and ± 1 V, are available for insertion into high impedances and 50-ohm inputs, respectively. The transition duration of the step is about 6 nanoseconds and it settles exponentially to 0.02 percent of the final value in less than 25 ns.

The NBS step generator was developed by Howard Schoenwetter, Donald Flach, and T. Michael Souders.

Nonaqueous Reference Electrode

An NBS/University of Texas team won an I-R 100 award for developing a new kind of reference electrode for measuring voltages in nonaqueous electrochemical systems. These measurements are important to industries such as battery manufacturers who use electrochemical techniques to research new materials for their products. Nonaqueous electrochemistry also is being used increasingly in the production of industrial chemicals, an example of where the new electrode's reproducible measurements can be an important factor in improving chemical process control and efficiency.

Previously, in the absence of a nonaqueous reference electrode, many industries have resorted to adapting electrodes intended for aqueous systems. Results often have been unsatisfactory.

There have been other industrial attempts to perfect a nonaqueous electrode, but limitations such as difficulty of use and lack of stability have hampered development. The NBS/Texas team, however, has overcome these hurdles and now offers a design that can be readily adapted for industrial use or for commercial production.

The electrode consists of a thin polymer film of polyvinylferrocene that has been electro-deposited on a platinum disk. The film is then treated with a crosslinking agent which, when thermally activated, stabilizes the film for use.

The device was developed by Rosanne Kannuck, Elmo Blubaugh, and Richard Durst of NBS, and Allen Bard and Pamela Peerce-Landers of the University of Texas.

Image Processing Engine

Ernest W. Kent, formerly of NBS, and James M. Herriman, Randall L. Luck, and Gerald S. Henrici of Digital/Analog Design Associates, Inc., won an I-R 100 award for the invention and development of an advanced parallel-architecture computer designed specifically for the high-speed processing of video images in "real time."

The Pipelined Image Processing Engine, modeled after processes in the human visual cortex, is expected to have application in a wide variety of advanced image-sensing equipment where continuous, real-time, processing is necessary, such as in machine vision systems for robots and robotic vehicles.

The computer handles the complex preprocessing of images from a digital video camera, performing hundreds of millions of calculations every second to manipulate raw visual images and generate all the information necessary for a vision system computer to recognize specific features such as texture, shade, the presence or absence of an edge, or motion at every point in a 256 by 256 "frame."

Its advanced features include a "multiple instruction-stream, multiple data-stream" capability that allows it to perform different operations on different regions of the same frame, depending on the nature of information at each point, and the ability to do a wide variety of motion-analysis and stereo operations. Other features include a sophisticated, graphics-oriented programming capability and a high-speed interface system that organizes the results of its analyses in a convenient form for the memory of another computer.

A commercial version of the device is being offered by Digital/Analog Design Associates, Inc., of New York. Kent now works for North American Philips Corporation at Philips Laboratories in Briarcliff Manor, NY.

Microscopic Reference Material

Standard Reference Materials are carefully prepared samples of materials of industrial or medical interest for which NBS certifies the values of certain physical or chemical properties. They are commonly used in labs throughout the world to assure the quality of measurements and scientific instrument performance.

NBS has received an I-R 100 award for the development of SRM 1960, 10-Micrometer Polystyrene Spheres, the first space-made product to be sold. The spheres are a nearly ideal micro-length standard to improve microscopic measure-

ments in electronics, medicine, and in the manufacture of finely ground products such as flour, cosmetics, paint pigments, and chemicals. The billions of tiny spheres, each of which measures about 1/2500th of an inch in diameter, were produced by Lehigh University and the National Aeronautics and Space Administration (NASA) aboard the space shuttle Challenger in April 1983 using a specially developed chemical process.

They were manufactured in space because earth-bound processes have not produced sufficiently uniform materials in usable quantities. When produced in a low-gravity environment, however, the polystyrene spheres grow uniformly in size and shape.

The new measurement standard was certified by NBS physicists Thomas R. Lettieri, Arie W. Hartman, and Gary G. Hembree, and coordinated by project manager Lee J. Kieffer (deceased) and Stanley D. Rasberry, chief of the NBS Office of Standard Reference Materials. Russell C. Obbink, NBS Research Associate from the American Society for Testing and Materials (ASTM), worked in the NBS laboratories and coordinated industry participation in the certification program.

John W. Vanderhoff, Fortunato J. Micale, and Mohamed S. El-Aasser of Lehigh's Emulsion Polymers Institute (Bethlehem, PA) and Dale M. Kornfield of NASA's Marshall Space Flight Center (Huntsville, AL) were in charge of producing the spheres used to make SRM 1960.